Check for updates

Received: 30 December 2022 | Revised: 26 December 2023 | Accepted: 28 January 2024

DOI: 10.1002/rob.22304

RESEARCH ARTICLE

WILEY

Nautilus: An autonomous surface vehicle with a multilayer software architecture for offshore inspection

Daniel F. Campos[1,2] | Eduardo P. Gonçalves[1,2] | Hugo J. Campos[2] | Maria I. Pereira[1,2] | Andry M. Pinto[1,2]

[1]Department of Electrical and Computer Engineering, Faculty of Engineering, University of Porto, Porto, Portugal

[2]INESC TEC, Porto, Portugal

Correspondence
Daniel F. Campos, Department of Electrical and Computer Engineering, Faculty of Engineering, University of Porto, Porto, Portugal.
Email: daniel.f.campos@inesctec.pt

Funding information
Horizon 2020 Framework Programme; Fundação para a Ciência e a Tecnologia; Portuguese Government, Grant/Award Numbers: SFRH-BD-144263-2019, 2021.05561.BD; European Union's Horizon 2020, Grant/Award Number: 871571

Abstract

The increasing adoption of robotic solutions for inspection tasks in challenging environments is becoming increasingly prevalent, particularly in the offshore wind energy industry. This trend is driven by the critical need to safeguard the integrity and operational efficiency of offshore infrastructure. Consequently, the design of inspection vehicles must comply with rigorous requirements established by the offshore Operation and Maintenance (O&M) industry. This work presents the design of an autonomous surface vehicle (ASV), named Nautilus, specifically tailored to withstand the demanding conditions of offshore O&M scenarios. The design encompasses both hardware and software architectures, ensuring Nautilus's robustness and adaptability to the harsh maritime environment. It presents a compact hull capable of operating in moderate sea states (wave height up to 2.5 m), with a modular hardware and software architecture that is easily adapted to the mission requirements. It has a perception payload and communication system for edge and real-time computing, communicates with a Shore Control Center and allows beyond visual line-of-sight operations. The Nautilus software architecture aims to provide the necessary flexibility for different mission requirements to offer a unified software architecture for O&M operations. Nautilus's capabilities were validated through the professional testing process of the ATLANTIS Test Center, involving operations in both near-real and real-world environments. This validation process culminated in Nautilus's reaching a Technology Readiness Level 8 and became the first ASV to execute autonomous tasks at a floating offshore wind farm located in the Atlantic.

KEYWORDS
field robotics, inspection robots, robotics, systems design

This is an open access article under the terms of the Creative Commons Attribution-NonCommercial-NoDerivs License, which permits use and distribution in any medium, provided the original work is properly cited, the use is non-commercial and no modifications or adaptations are made.
© 2024 The Authors. *Journal of Field Robotics* published by Wiley Periodicals LLC.

1 | INTRODUCTION

The offshore energy production industry is growing with offshore wind farms being regarded as one of the potential main energy suppliers in the near future (Lee et al., 2016). Thus, it is crucial to inspect and maintain all infrastructures to ensure the best performance and efficiency. As such, Operation and Maintenance (O&M) is becoming an emerging necessity that currently is mostly human based and demands the use of a vast amount of resources (e.g., human assets, support vessels, etc.) which leads to higher inspection costs and safety risks.

Currently, it is no longer uncommon to find examples of robotic applications in the most challenging environments, such as underwater (Plueddemann et al., 2012), maritime (Campos, Pereira, et al., 2021), or aerial (Wang, Zhang, et al., 2019) domains. Moreover, unmanned vehicles, namely, Unmanned Aerial Vehicles (UAVs), Autonomous Surface Vehicles (ASVs), Remotely Operated Vehicles (ROVs), and Autonomous Underwater Vehicles, are being developed and deployed to perform O&M activities, such as autonomous navigation (Cui et al., 2021), mapping (Teng et al., 2021), underwater manipulation (Silva et al., 2022), or visual inspection (Leite & Pinto, 2024; Pinto & Matos, 2020). Thus, autonomous systems must be compliant with the singularities of the environment they are exposed to. Not only must the sensors cope with the conditions of the environment and with the tasks to be performed, but also the actuators should take into account the dynamics of movements the agent is subject to.

Nautilus was specifically designed to operate in offshore O&M environments, adhering to the limitations imposed on small boats, with a maximum significant wave height of 1.5 m. The challenging environmental conditions in these locations restrict inspection activities to narrow operation windows, particularly during the optimal period between June and August, with an average operation window length of 2 days (Silva & Estanqueiro, 2013). The vehicle presents a compact hull, measuring 3.0 m in length and weighing 130 kg, capable of navigating in moderate sea states up to Douglas Sea State 4 with an autonomy of approximately 3 h. Its modular hardware and software architecture readily adapts to mission-specific requirements, facilitating the integration of various sensors and payload configurations. Nautilus seamlessly communicates with a Shore Control Center (SCC) and beyond visual line-of-sight (BVLOS) control scenarios, employing a 2.4-GHz radio controller with a range of 20 km. The ASV's comprehensive sensor payload encompasses Global Positioning System (GPS), Inertial Measurement Unit (IMU), Light Detection and Ranging (LiDAR) Multibeam Echosounder (MBES), visual, and thermal cameras, enabling multiple O&M inspection tasks. Furthermore, the software architecture, the Multilayer Universal Software Architecture (MUSA), is presented. It is a skills-based architecture that aims to provide an adaptable platform to describe a mission as a set of tasks with different skills performing several actions, that can be transversal to several types of autonomous assets.

Therefore, the main contributions of this paper include:

- Design of a compact ASV with a multidomain sensor payload and capable of operating in offshore conditions and BVLOS. Its fully electric design contributes to an environmentally sustainable technology aiming to reduce the need for traditional vessels, thereby minimizing CO_2 emissions.
- An integrated and adaptable multilayer software architecture designed for O&M operations. The architecture comprises four distinct levels—mission, task, skill, and action—designed to ease the programming task for developers and engineers, making it faster and simpler to program different autonomous agents, while avoiding code redundancy. Additionally, a publicly accessible repository is provided, showcasing a practical implementation of the bottom three levels—task, skill, and action—of the proposed architecture, focused on a positioning algorithm for maritime applications.
- Extensive experiments in near-real and offshore scenarios to demonstrate Nautilus' ability to perform multiple inspection tasks simultaneously, such as transition piece and seabed mapping or scour protection inspection, and the deployability from the port or a vessel in offshore.
- Nautilus was the first ASV to operate autonomously at a floating offshore wind farm located in the Atlantic, namely, the WindFloat Atlantic (WFA) wind farm owned by Ocean Winds. A video of the operation can be found at the following link http://tinyurl.com/nautilus-off.

The document is arranged as follows: in Section 2 it is presented the related work with a brief overview of the current ASV technologies and of skill-based software approaches available in the literature. In Section 3, the Nautilus' concept and hardware architecture are presented, as well as MUSA is described. Section 4 depicts the Nautilus real-world experiments and data with different conditions, namely, in a near-real and a real scenarios. At last, Section 5 provides some final remarks and conclusions.

2 | RELATED WORK

The inspection of offshore wind farms is a harsh task with multiple operation constraints, such as a maximum wave height of 1.5 m for using a small boat on site or wind of at most 5 m s^{-1} to climb the met masts (Silva & Estanqueiro, 2013). The current procedures use ROVs and divers for observing the subsea structures, and rope access and teleoperated UAVs for the aerial parts. The wind turbine infrastructure state is usually assessed through NonDestructive Techniques (NDTs), such as visual inspection, ultrasonic testing, infrared (IR) thermography, LiDAR mapping or electromagnetic testing (Civera & Surace, 2022). Therefore, the offshore wind energy industry would benefit from the employment of autonomous vehicles for monitoring and inspection endowed with multimodal sensors to create cost-effective O&M strategies and ensure repeatability and less risk for human life (Albrechtsen, 2012).

In particular, the use of ASVs can be helpful due to the capability to perceive multidomain data. Papadopoulos et al. (2014)

15564967, 2024, 4, Downloaded from https://onlinelibrary.wiley.com/doi/10.1002/rob.22304 by SEA ORCHID (Thailand), Wiley Online Library on [16/02/2026]. See the Terms and Conditions (https://onlinelibrary.wiley.com/terms-and-conditions) on Wiley Online Library for rules of use; OA articles are governed by the applicable Creative Commons License

TABLE 1 Comparison of available ASVs.

ASV	Hull type	Dimensions (m)	Douglas Sea State	GPS	IMU	LiDAR	Sonar	Visual camera	Thermal camera
ROAZ (Ferreira et al., 2009)	Catamaran	4.5 × 2.2	3	✓	✓	×	✓	×	✓
SENSE (Campos et al., 2022)	Catamaran	1.5 × 1.1	2	✓	✓	✓	✓	✓	×
HydroCat-180[2]	Catamaran	5.5 × 2.5	5	✓	✓	✓	✓	✓	×
SCOUT (Papadopoulos et al., 2014)	Monohull	3.0 0.5	2	✓	✓	✓	✓	×	×
ASAROME (Plumet et al., 2015)	Monohull	3.6 (length)	2	✓	✓	×	✓	✓	×
Roboat (Wang, Gheneti, et al., 2019)	Monohull	0.9 0.5	2	✓	✓	✓	×	✓	×
DriX (Eudeline, 2009)	Monohull	7.7 0.8	5	✓	✓	×	✓	×	×
Aragon (Han et al., 2020)	Monohull	8.0 2.4	5	✓	✓	✓	×	✓	×
Kongsberg Geoswath Plus[4]	Monohull	1.7 0.8	2	✓	✓	×	✓	×	×
Teledyne Z-Boat 1800RP[1]	Monohull	1.8 × 1.0	2	✓	✓	✓	✓	✓	×
C-Worker 7[3]	Monohull	7.5 × 2.3	5	✓	✓	×	✓	✓	✓
Nautilus	Monohull	3.0 × 1.4	4	✓	✓	✓	✓	✓	✓

Abbreviations: ASV, autonomous surface vehicle; GPS, Global Positioning System; IMU, Inertial Measurement Unit; LiDAR, Light Detection and Ranging.

use a kayak with a 3-m length equipped with GPS, IMU, and doppler velocity log as navigation sensors, and five 2D laser scanners, two of them mounted on a rotating shaft, and an imaging sonar, used for perceiving the surface and underwater domains and reconstructing partially submerged structures. Plumet et al. (2015) present a sailing boat hardware and software architecture for autonomous navigation within the framework ASAROME. It is equipped with a visual camera, sonar, hydrophones, anemometer, GPS, and IMU for perceiving the scenario and is capable of detecting obstacles and path planning, where each model was tested independently on a lake. Campos et al. (2022) developed the SENSE a modular catamaran-like ASV capable of gathering multi-domain data using a 3D LiDAR and an MBES, suitable to operate with favorable weather conditions and in calm waters. Multidomain commercial solutions are starting to emerge, namely, the Teledyne Z-Boat 1800RP[1] and the HydroCat-180[2] which gather data from a sonar and a 3D LiDAR for coastal and offshore applications, respectively. Another example is the C-Worker 7[3] which is designed for offshore inspections and acquires data from a sonar, and visual and thermal cameras. Nevertheless, the use of ASVs for single-domain applications is still the most commonly used in both academia and industry. Commercial solutions like Kongsberg Geoswath Plus USV,[4] or DriX (Eudeline, 2009) are becoming more widespread for bathymetric surveys. In the academia, the most common applications found are ASVs for underwater surveys, such as the ROAZ proposed by Ferreira et al. (2009). Some applications using aerial data are also available, such as the Aragon USV introduced by Han et al. (2020) for collision avoidance or Wang, Gheneti et al. (2019) and Wang et al. (2018) Roboat designed for operating in dynamic GPS-attenuated urban waterways, that utilizes LiDAR, camera, and IMU for localization. The Nautilus stands out for its compact design, enabling operation in moderate sea conditions while capturing multidomain data. Featuring smooth maneuverability, BVLOS capabilities, and ease of transport and deployment, the Nautilus facilitates the simultaneous execution of multiple inspection tasks, including visual inspection, IR thermography, LiDAR mapping, and underwater surveying. Table 1 summarizes the key specifications of the aforementioned ASVs, highlighting the Nautilus's capability to handle the expected sea conditions, namely, Douglas Sea State 4, while being the smallest vehicle encompassing a comprehensive sensor payload for NDT inspections in both surface and underwater domains, namely, GPS, IMU, LiDAR, Sonar, and Visual and thermal cameras.

Furthermore, to ensure an architecture that can be transversal to multiple operations and scenarios, the pursuit of a layered architecture for robot control is crucial, either because researchers need to add complexity to previously designed systems, extend their functionalities, add flexibility, or even to make the programming task less burdensome. Brooks (1986) proposed a layered control system for mobile robots. His goal was to increase the level of competence of robots. Higher layers of the architecture could take control over lower levels, injecting inputs signals and inhibiting their outputs. Hasegawa et al. (1992) defined skills as the building blocks of robot tasks. They proposed a model that made skills independent from the manipulator configuration, leaving low-level control to skill primitives, below skill level.

[1]Teledyne, 2023. *Z-Boat 1800RP*. URL: https://tinyurl.com/z-boat1800rp.
[2]Seafloor Systems, 2023. *HydroCat-180*. URL: https://tinyurl.com/seafloorsystems-hydrocat180.
[3]L3Harris, 2023. *C-Worker 7*. URL: https://tinyurl.com/c-worker7-datasheet.
[4]Kongsberg, 2023. *Geoswath Plus USV*. URL: https://tinyurl.com/57yws7zx.

15564967, 2024, 4, Downloaded from https://onlinelibrary.wiley.com/doi/10.1002/rob.22304 by SEA ORCHID (Thailand), Wiley Online Library on [16/02/2026]. See the Terms and Conditions (https://onlinelibrary.wiley.com/terms-and-conditions) on Wiley Online Library for rules of use; OA articles are governed by the applicable Creative Commons License

The pivotal point to the definition of a hierarchized skill-based architecture was the work by Pedersen et al. (2016), where a conceptual model of skills for industrial robots was proposed, directed at reducing the complexity of the programming labor. Their goal was to allow nonexperts to program robots to perform complex tasks, relieving the complexity burden that such a job used to carry. They divided the operation of industrial robots into three distinct layers: tasks, skills, and device primitives. Each layer of the architecture communicated with its lower layer, in a hierarchical fashion. A task was, therefore, composed of a sequence of preprogrammed skills, and defined the complex operations of the autonomous agents. Nevertheless, its task execution speed remains a significant limitation, where human workers or robots specifically designed for the same purpose offer superior performance. The work has since been a reference for researchers in the field, with a highlight on human–robot collaboration (Kyrarini et al., 2019; Schou et al., 2018). Huang et al. (2018) proposed a skill-based programming system for robotic furniture assembly. They divided skills into primitive skills and compound skills, with the latter being a sequence of several skills. They argued this approach would facilitate software reusability, as it allowed developers to group several preprogrammed skills, adding complexity to the assembly operation. Regarding mobile robots, not much research is available to the scientific community in the context of skill-based approaches. The work by Leite et al. (2018) is one of the scarce examples available. They implemented a fault-detecting skill, expanding the conceptual model of skills for industrial robots, so that a safety monitoring module could be incorporated. It was later tested in an ASV, in the form of a fault-detecting GoTo skill. Albore et al. (2021) developed a skill-based software architecture with resilient behaviors that could accommodate sensor failures and communication losses in UAV operations. The architecture is divided into a decision, a skill, and a functional layer. The former was responsible for defining which skills were to be executed and was implemented in the form of a Behavior Tree. Skills were chosen through motion and perception skillsets, and use and send information from and to the functional layers. The MUSA expands Pedersen et al. (2016) architecture to contribute with a flexible structure composed of four levels (mission, task, skill, and action) that is transversal to several vehicles and systematizes the mission to an easily reconfigurable architecture while maintaining the performance of tailor-made robotic tasks. It aims to provide a development standard for inspection missions, mainly with maritime robots.

3 | NAUTILUS ASV PLATFORM

3.1 | Concept

Inspection of offshore infrastructures usually demands a robust platform with distinct sensor payloads for each application, such as an MBES for surveying scour protection or a visual camera for acquiring geo-tagged images of flaws in the structure. In this scenario, the interventions are highly weather-constrained with a limited operational time window.

The Nautilus, depicted in Figure 1, is an ASV designed for patrolling and the inspection of maritime scenarios, such as harbors and offshore wind farms. It uses multidomain perception sensors, namely, MBES, LiDAR, and visual and thermal cameras. This payload allows one to reconstruct the environment, inspect faulty structures, and extend the vehicle situational awareness capabilities. Navigation sensors, in particular GPS and IMU, are also available for localizing the vehicle and performing autonomous operations.

The ASV design provides a stable and robust platform with a monohull configuration, while maintaining a small footprint to be easy to transport and deploy. The hull design as well as the navigation payload allows it to operate within the range of Sea State 4, up to



FIGURE 1 Nautilus ASV operating in Viana do Castelo. ASV, autonomous surface vehicle.

15564967, 2024, 4, Downloaded from https://onlinelibrary.wiley.com/doi/10.1002/rob.22304 by SEA ORCHID (Thailand), Wiley Online Library on [16/02/2026]. See the Terms and Conditions (https://onlinelibrary.wiley.com/terms-and-conditions) on Wiley Online Library for rules of use; OA articles are governed by the applicable Creative Commons License

2.5 m maximum wave height, in the Douglas sea scale (Curto et al., 2021). Thus, Nautilus works within the expected operation window on offshore wind farms for boats with small hulls, that is, a maximum wave height of 1.5 m. Nautilus' modular hardware architecture allows one to easily include, remove or replace sensors according to the operation requirements. The current design provides heterogeneous data from the surface and the underwater domains that can be visualized on an SCC through wireless fidelity (Wi-Fi) communication (Neves et al., 2023). This SCC also enables the definition, supervision and control of the vehicles' missions. Moreover, the ASV can be also teleoperated with BVLOS capabilities through a 2.4-GHz radio controller with a 20-km range.

3.2 | Hardware design

3.2.1 | Hardware description

The Nautilus is a compact vessel with a 3.0-m length and approximately 130 kg, Figure 2. It has a monohull configuration built using glass reinforced plastic composite sandwich making up a weight of approximately 45 kg, and a net buoyancy of 250 kg. It is equipped with several linking unions, where the modules boxes can be attached, and maritime-grade stainless-steel fixation plates to support the surface sensors. The underwater sensors can be placed through a moon pool hatch placed on the center of the hull with a size of 373 373 mm. Its modules are powered through a 24-V and 150-Ah LiFePO4 battery, stored in a *Peli* case. This provides an autonomy of approximately 3 h with the current payload, considering the motors are working around half-throttle. The energy module can be easily replaced or charged externally without requiring to open the case.

Moreover, Nautilus has a differential drive configuration via two brushless outboard motors placed at the stern of the hull, equivalent to two 3 hp petrol outboards, controlled by a commercial vedder's electronic speed controller solution. Each motor produces a propulsive power of 520 W with a power consumption of at most 1100 W. This configuration allows Nautilus to reach velocities up to 3 m s^{-1}.

As for the current sensor payload, it provides multidomain and navigational data, being composed of:

- A GPS, with real-time kinematic (RTK) technology at a rate of 3 Hz. The accuracy with Global Navigation Satellite System is 1.5 m and with RTK 0.01 m. It provides the localization of the vehicle and allows one to geo-tag inspected flaws.
- A nine degrees-of-freedom IMU that provides the attitude of the vehicle, the angular velocity, and linear acceleration with a rate of 20 Hz and an East-North-Up referential. The sensor fusion provides an error of 0.2° root mean square in roll and pitch, and 1.0° for yaw. It can be employed for the vehicle localization and the perception data alignment.
- A 3D LiDAR, with 128-channel LiDAR, a range of up to 200 m, a 360° × 45° Field of View (FoV) and a rate of 10 Hz. The sensor has a mean range error of 2.5 cm. It is applied to reconstruct the surface environment, detect nearby obstacles, and navigate near structures.
- Two visual cameras, with a 12.5-mm lens, a resolution up to 1440 1080, a rate of 30 Hz and external triggering. These sensors are synchronized via the external trigger allowing them to be used for stereo perception with a baseline of 50 cm, capable of tracking surrounding elements, detecting structural flaws, providing stereoscopic information, and supplying visual data for BVLOS teleoperation.
- A thermal camera, with a 13-mm lens, a resolution of 336 256, and a rate of 30 Hz. It provides thermographic data required for inspection and detection of flaws in offshore structures and, alongside the LiDAR, facilitates night operations.
- An MBES, with a frequency of 260 kHz, range up to 100 m, an angular FoV of 120°,° and a 20-Hz rate. The sensor has a range resolution of 0.2% of the range. It allows one to inspect underwater structures, create bathymetry information, and geo-localize submerged structures.

A sample of the navigation data (GPS and IMU) taken in one of the trials is depicted in Figure 3, where it can be observed the vehicle trajectory, represented by the green line, an attitude meter, placed on

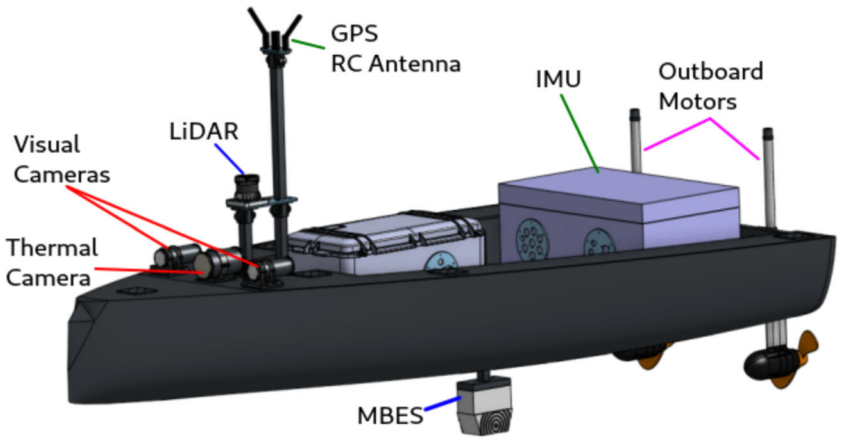


FIGURE 2 Nautilus CAD with the sensor payload attached. The blue, red, and green lines are distance, imaging, and navigation sensors, respectively. The pink lines are the actuators. CAD, computer-aided design; GPS, Global Positioning System; IMU, Inertial Measurement Unit; LiDAR, Light Detection and Ranging; MBES, Multibeam Echosounder; RC, remote control.

15564967, 2024, 4, Downloaded from https://onlinelibrary.wiley.com/doi/10.1002/rob.22304 by SEA ORCHID (Thailand), Wiley Online Library on [16/02/2026]. See the Terms and Conditions (https://onlinelibrary.wiley.com/terms-and-conditions) on Wiley Online Library for rules of use; OA articles are governed by the applicable Creative Commons License

the bottom that represents the vehicle roll, pitch and yaw, and an image, retrieved by the visual camera.

Figure 4 depicts a sample of the perception data. It provides visual information through the cameras (right and left) with different perspectives to be able to perform stereo matching. Nevertheless, this information is highly constrained by the lighting conditions and fog. The LiDAR and the MBES provide distance information using IR and sonar technology, respectively, being less susceptible to environmental changes. The thermal camera provides an IR image which allows one to retrieve the structures' temperature and operate in low-lighting conditions.

Table 2 depicts a summary of the Nautilus characteristics.

3.2.2 | Hardware architecture

Nautilus hardware is distributed between two watertight cases containing: energy module, and perception, navigation, and communication (PNC) module. The first is solely composed of the battery with the integrated Battery Management System and the system power cut-off system. The second is arranged into distinct submodules that create the interfaces with the sensors and actuators, define the internal and external communications, and execute the defined mission. All physical interfaces between modules and external connections are made through side panels adaptable to suit the required connectors.

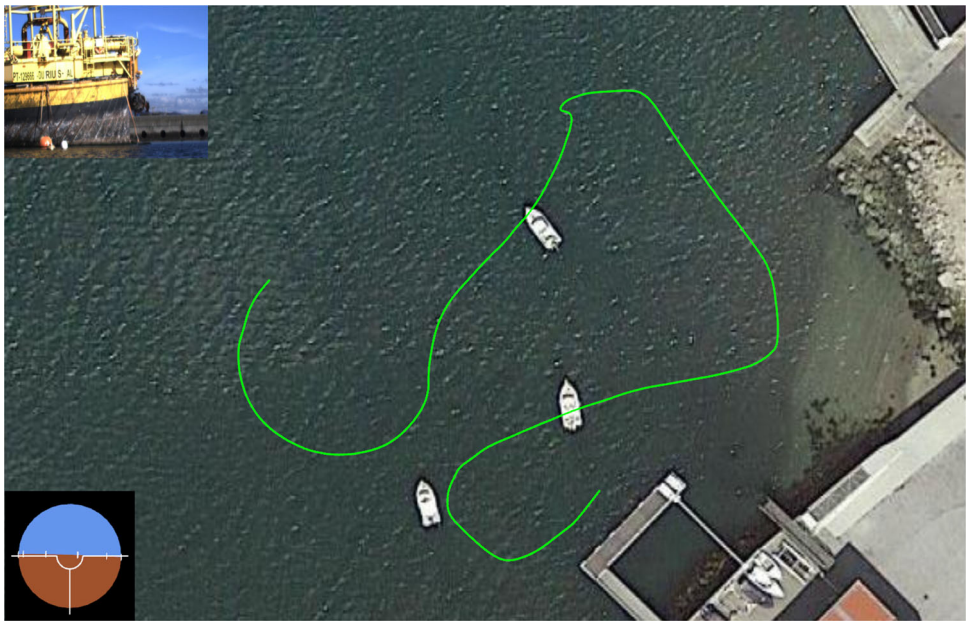


FIGURE 3 Navigation data from the Nautilus. The green line corresponds to the GPS positions and the attitude meter depicts the current roll, pitch, and yaw of the vehicle. GPS, Global Positioning System.

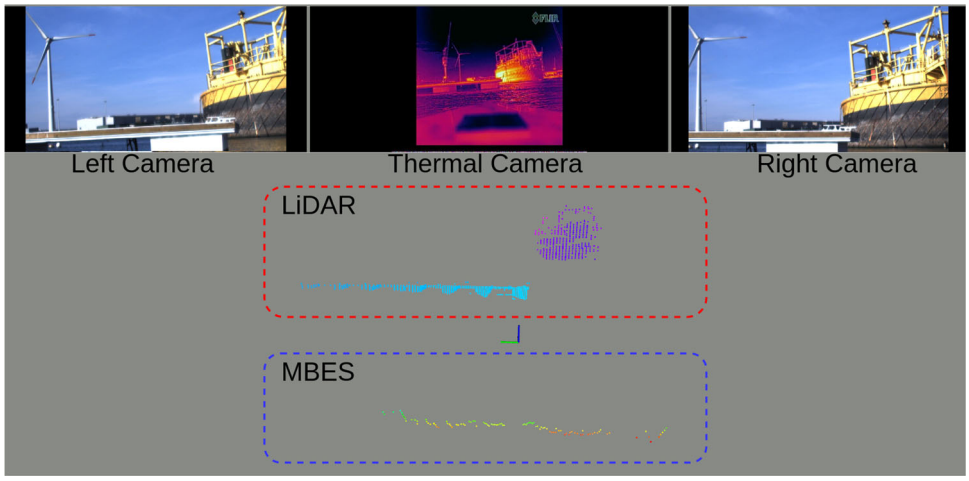


FIGURE 4 Nautilus perception data gathered in Viana do Castelo. LiDAR, Light Detection and Ranging; MBES, Multibeam Echosounder.

15564967, 2024, 4, Downloaded from https://onlinelibrary.wiley.com/doi/10.1002/rob.22304 by SEA ORCHID (Thailand), Wiley Online Library on [16/02/2026]. See the Terms and Conditions (https://onlinelibrary.wiley.com/terms-and-conditions) on Wiley Online Library for rules of use; OA articles are governed by the applicable Creative Commons License

TABLE 2 Technical specifications of the Nautilus.

Characteristics	Specifications
Dimensions (*L W H*)	3.0 m 1.4 m 1.5 m
Total weight	~130 kg
Available payload	~120 kg
Moon pool size	373 mm 373 mm
Drive mode	Differential drive
	Outboard motors
Maximum speed	3 m s^{-1}
On-board sensors	Navigation: GPS, IMU
	Perception: 3D LiDAR, MBES, visual
	Cameras (×2), thermal camera
Power supply	$LiFePO_4$ 24 V@150 Ah
Power consumption (maximum)[a]	~2700 W
Operation time	~3 h
Douglas sea scale	4 (up to 2.50 m)

Abbreviations: GPS, Global Positioning System; IMU, Inertial Measurement Unit; LiDAR, Light Detection and Ranging; MBES, Multibeam Echosounder.

[a]Maximum power consumption values for each individual component were considered to estimate the overall energy consumption.

The PNC module, as depicted in Figure 5a, is divided into two submodules, navigation and communication (NavCom), and perception. Each one is endowed with a processing unit, linked through a gigabit local network.

The NavCom submodule is designed as the master processing unit to ensure the safety by design, where a critical fault from the navigation components halts the vehicle, whilst a defect from the perception parts allows the vehicle to return to base. As such, the NavCom creates the internal and external communications, controls the outboards, acquires navigational data and executes the teleoperation and autonomous navigation procedures, Figure 5b. This submodule uses an embedded computer as the processing unit that acquires the IMU data and communicates through Mavlink to acquire the RC and GPS inputs, Gigabit Ethernet to create the local network and Wi-Fi to communicate with the SCC.

The perception submodule is designed for higher computational capacity to withstand the larger data acquisition and processing requirements. This is connected to the NavCom through the local network and uses a laptop as a processing unit. As such this unit is responsible for acquiring data from the perception sensors, filtering the data, perform skills to increase the situational awareness, such as visual odometry (Agostinho et al., 2022), obstacle detection (Duarte et al., 2022), and inspection methodologies, for example, multidomain mapping (Campos et al., 2020). Moreover, this submodule logs all the data retrieved by Nautilus, that can be accessed and retrieved via Wi-Fi.

All communications, internal and external, use distinct protocols being connected as depicted in Figure 6, where all timestamps between assets are synchronized using a Network Time Protocol designed to perform well with intermittent network connections, and heavily congested networks, having a sub-microsecond accuracy. Both processing units are connected through ethernet and use the robot operating system (ROS) framework (Quigley et al., 2009) to create the data bridges between them, while defining the NavCom as the master unit and establishing an external bridge connection through a Wi-Fi extender. The sensors are linked through their predefined interface, either ethernet, power over ethernet (PoE) or serial. The Mavlink autopilot is equipped with a redundant IMU and allows one to retrieve the telemetry from the vehicle, acquiring the GPS data and synchronizing through a Wi-Fi link with the RTK base station. Moreover, the autopilot also provides the communication between the BVLOS RC command and the navigation processing unit. This BVLOS system communicates through a 2.4-GHz link and allows not only to control the vehicle, but also to monitor the telemetry and stream a visual image using the Mavlink protocol.

This hardware architecture endows Nautilus with a modular framework capable of adapting distinct sensors and executing different tasks adapted to the designed mission. With the current design, the ASV is capable of performing skills like mapping and localization near structures (Claro et al., 2020), obstacle avoidance (Campos et al., 2019), autonomous docking (Pereira et al., 2021), or object tracking (Wolf et al., 2010). Thus, it demands a substantial flexibility from the software architecture to adapt to the different hardware and skills that the ASV is able to fulfill.

3.3 | Multilayer universal software architecture

Offshore O&M presents challenging conditions to the autonomous agents that perform them. The different domains of operation—air, surface, and underwater—expose autonomous vehicles to environments with the most distinct dynamics and constrains. Most of the times, new robots are reprogrammed from scratch, discarding work that could potentially serve the same purpose. Aiming at reducing waste of resources and the need to redo redundant work, skill-based approaches come into hand. With a focus on industrial robotics, such architectures usually divide the architecture into several layers. The bottom layer, composed of actions or primitives, interconnects the hardware to the decision-making layer, where skills sit. This way, skills output data that are independent of the hardware, creating a level of abstraction that is much desired when software reusability is wanted. On top of the skill level, a task level usually concatenates skills in a sequentially arranged fashion, allowing for distinct complex operations to be run one after the other.

Mobile robot applications of such architectures are, however, still very scarce. The MUSA aims at filling that void. Its main goal is to ease the programming task of mobile robots, and it tackles challenges, such as software portability and reusability, and data source agnosticism. In other words, it aspires at making the code interchangeable and independent from the protocol that drives data from sensors and to actuators. Thus, the underlying principle of

15564967, 2024, 4, Downloaded from https://onlinelibrary.wiley.com/doi/10.1002/rob.22304 by SEA ORCHID (Thailand), Wiley Online Library on [16/02/2026]. See the Terms and Conditions (https://onlinelibrary.wiley.com/terms-and-conditions) on Wiley Online Library for rules of use; OA articles are governed by the applicable Creative Commons License

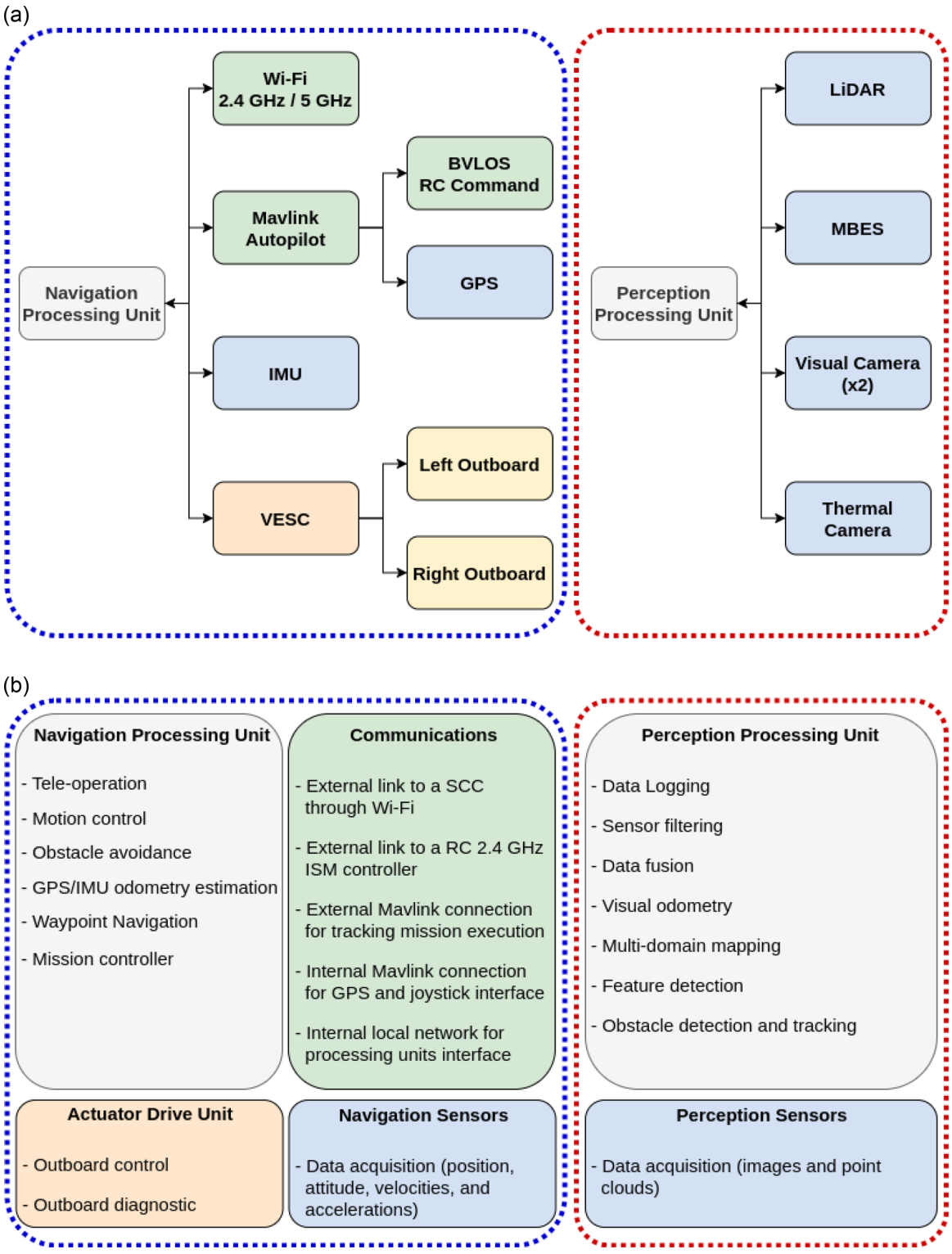


FIGURE 5 Nautilus hardware and functionalities layout. The blue and red dashed boxes are the navigation and communication, and perception submodules, respectively. The gray, green, blue, orange, and yellow boxes are the processing units, communications, sensors interfaces, actuator drive units, and actuators, correspondingly. (a) Nautilus PNC module structure and (b) Nautilus functionalities layout. BVLOS, beyond visual line-of-sight; GPS, Global Positioning System; IMU, Inertial Measurement Unit; LiDAR, Light Detection and Ranging; MBES, Multibeam Echosounder; PNC, perception, navigation, and communication; RC, remote control; SCC, Shore Control Center; Wi-Fi, wireless fidelity.

15564967, 2024, 4, Downloaded from https://onlinelibrary.wiley.com/doi/10.1002/rob.22304 by SEA ORCHID (Thailand), Wiley Online Library on [16/02/2026]. See the Terms and Conditions (https://onlinelibrary.wiley.com/terms-and-conditions) on Wiley Online Library for rules of use; OA articles are governed by the applicable Creative Commons License

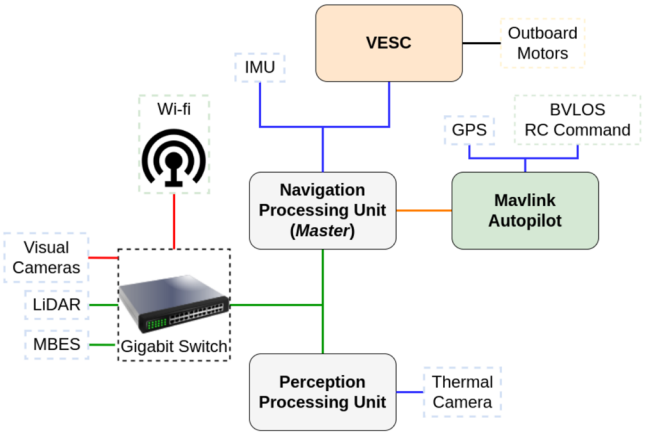


FIGURE 6 Nautilus internal and external communication links. The red, green, blue, orange and black lines represent the PoE, ethernet, serial, Mavlink and power outputs. BVLOS, beyond visual line-of-sight; GPS, Global Positioning System; IMU, Inertial Measurement Unit; LiDAR, Light Detection and Ranging; MBES, Multibeam Echosounder; RC, remote control; Wi-Fi, wireless fidelity.

MUSA is to foster software portability and establish an abstraction from the hardware in the control loop, where it can work stand-alone or be integrated into existing operating systems for robots, such as ROS and ROS2. A level of abstraction between layers that do not need to share information is also desired. That said, MUSA has to fulfill the following requirements:

- Each level of the hierarchy has to share information with the level atop or beneath it.
- A templated backbone for each level of the hierarchy must provide a mechanism that encompasses the basic operation of each element of that level.
- Every level has to be agnostic to the levels within reach, meaning each component of the hierarchy might be swapped for a more (or less) complex component, without loss of the system's functionality.

MUSA provides an architecture that can cope with complex O&M operations. It is composed of four levels: a Mission ($\mathcal{M}$), a Task ($\mathcal{T}$), a Skill ($\mathcal{S}$), and an Action ($\mathcal{A}$) level. This creates a hardware abstraction layer which separates from conventional architectures that are usually dependent on the autopilot in use. MUSA is designed to be able to cope with any hardware structure treating each dependency at the lower level of the architecture, the action layer.

The actions are closely related to hardware, they are responsible for turning information into commands that the hardware level, through its drivers, can interpret. A skill, $\mathcal{S}$, used in certain domains and environments can only depend on specific actions that are physically viable for the robot hardware and the operations to be performed. The skills add functionalities to a robot and are defined as a sequence of individual and self-contained actions. Having some sort of control process, they interpret information from the environment, collected by sensors, and make decisions. Thus, $\mathcal{S}$ can be seen as a set of n actions:

$$\mathcal{S} = \{\mathcal{A}_1, ..., \mathcal{A}_n\}, \quad (1)$$

$\mathcal{S}$ can be either persistent, that is, runs continuously in the background parallel to other skills until the task is stopped (e.g., odometry), or volatile, that is, runs once until the goal condition is reached (e.g., the positioning system). To avoid execution repetitions, persistent skills can be shared between tasks. Programming at this level requires a comprehensive knowledge of the operation to be conducted. It is also required that the dynamics and limitations of the domain to which the skill is to be applied are taken into account. It is at this level that information is turned into commands to be fed into the action layer. Therefore, routines such as motion planning, motion execution, and obstacle avoidance should be implemented at the skill level.

MUSA starts to differ from the already existing skill-based approaches at the task level. Unlike previous works, tasks are defined, not as a sequence of skills, but as a set of skills, which might be organized either sequentially, concurrently, or as a combination of both. Hence, tasks are a set of m skills planned to overcome a specific goal, that is,

$$\mathcal{T} = \{\mathcal{S}_1, ..., \mathcal{S}_m\}. \quad (2)$$

They also define input parameters for skills. Unlike statically placed industrial robots, mobile robots might have to perform several skills concomitantly (e.g., hoovering while a manipulator performs an operation). With this approach, MUSA takes advantage of concurrency, meaning mobile robots can benefit from skills that execute at the same time.

Above the task level, it is proposed a Mission layer, defined as a concatenation of tasks that are, again, run sequentially. Missions further extend the applicability of the proposed architecture, allowing for high-level programming of tasks, by simple definition of parameters. Thus, it can be defined as the set of k tasks:

$$\mathcal{M} = \{\mathcal{T}_1, ..., \mathcal{T}_m\}. \quad (3)$$

Upon the successful completion of all k tasks $\mathcal{T}$, it can be guaranteed that $\mathcal{M}$ was also successfully concluded. Nonetheless, these tasks are not exclusive to only mission, that is, two different missions, $\mathcal{M}_1$ and $\mathcal{M}_2$, can share the same task $\mathcal{T}$ or, even, being defined by the same set of tasks.

A visual representation of MUSA is depicted in Figure 7. To better understand the division, one can picture the scenario in which an ASV has to inspect an offshore wind farm autonomously. The whole inspection operation composes the entire mission, which can be broken into smaller operations—tasks—such as the inspection of individual wind turbines. The inspection of each wind turbine requires the ASV to be able to perform navigation skills, such as reaching a location and hovering around a fixed point. Skills send velocity commands to actions, which convert that information into commands for the ASV motors. Zooming in on each individual element of every layer (an individual mission, task, skill, or action), one can find that the main workflow follows a similar sequence, which goes as follows:

1. Upon start, an initialization routine is called. It is responsible for checking if the preconditions for the element's normal execution

15564967, 2024, 4, Downloaded from https://onlinelibrary.wiley.com/doi/10.1002/rob.22304 by SEA ORCHID (Thailand), Wiley Online Library on [16/02/2026]. See the Terms and Conditions (https://onlinelibrary.wiley.com/terms-and-conditions) on Wiley Online Library for rules of use; OA articles are governed by the applicable Creative Commons License

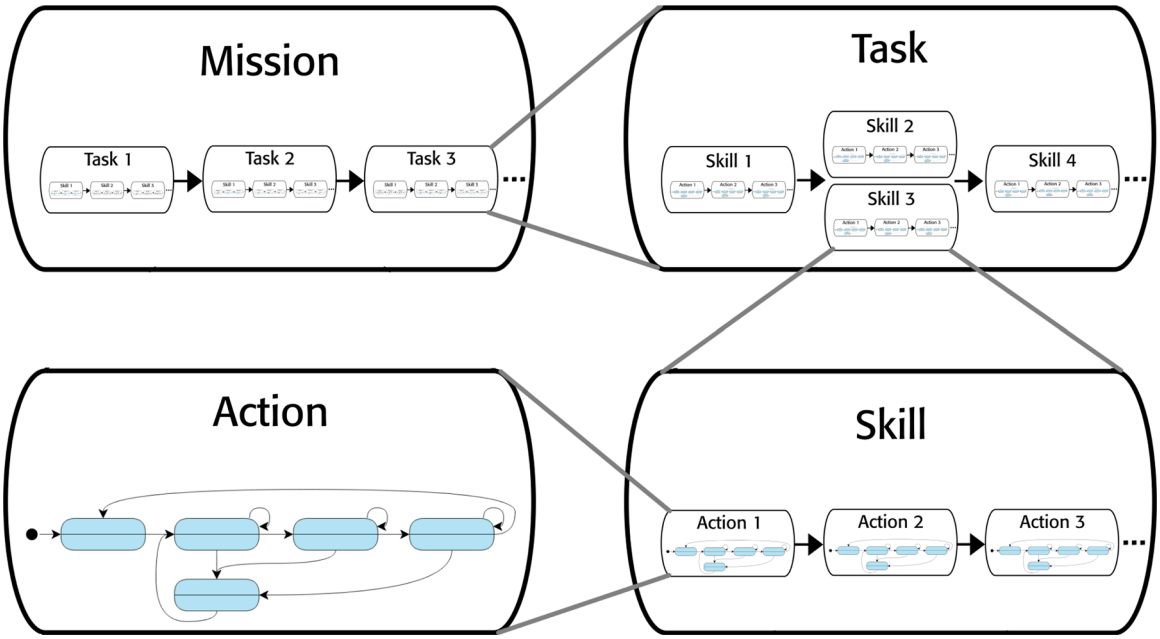


FIGURE 7 MUSA: The four layers that make the proposed architecture. MUSA, Multilayer Universal Software Architecture.

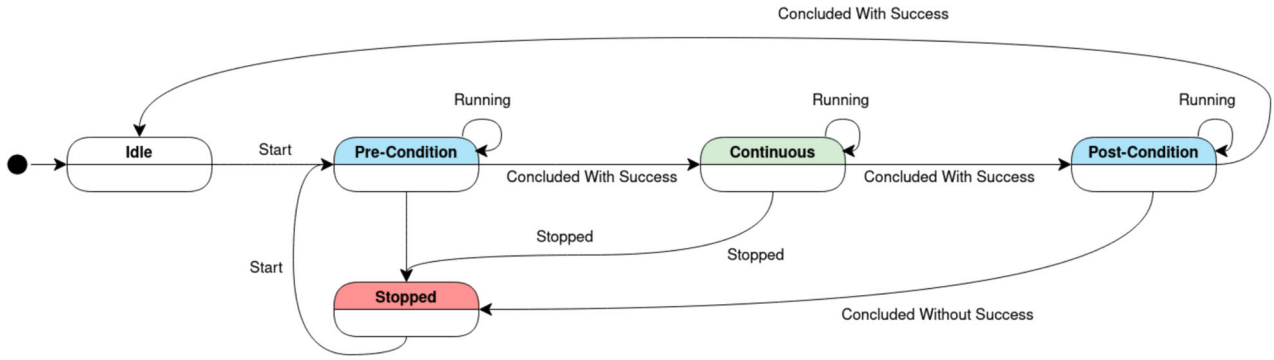


FIGURE 8 The state machine diagram of the execution of each individual element of the proposed architecture.

are met, and, if so, if it can proceed. Otherwise, the execution stops, returning an error.

2. The continuous execution routine is executed after the initialization procedures are completed. This routine is nonblocking, meaning its execution is triggered by an object of a layer on top of it or, if it is the case of the highest layer, at a certain rate. Once again, in case of failure, the execution is halted, requiring a new start command to be sent,
3. Before concluding the execution, a postcondition checking routine is called. It is responsible for checking the overall execution status of the process and, eventually, for sending the last commands to the action layer.

In case of failure of any of the aforementioned routines, the execution enters a failure routine, which halts the operations. A visual representation of the described workflow is illustrated in Figure 8, in the form of a state machine diagram.

3.3.1 | Inspection mission—Sample application

To illustrate the MUSA's functionality, a mission-level implementation was developed, depicted in Figure 9. It uses an event-based communication, namely, Qt's signals and slots,[5] to interchange information between layers and ROS (Quigley et al., 2009) messaging system to interface with hardware drivers. The architecture was fit into the ASV in the form of an autonomous inspection module for maritime environments, which can be divided as:

[5]Qt, 2023. *Signals & Slots*. URL: http://tinyurl.com/qtsigslot.

15564967, 2024, 4, Downloaded from https://onlinelibrary.wiley.com/doi/10.1002/rob.22304 by SEA ORCHID (Thailand), Wiley Online Library on [16/02/2026]. See the Terms and Conditions (https://onlinelibrary.wiley.com/terms-and-conditions) on Wiley Online Library for rules of use; OA articles are governed by the applicable Creative Commons License

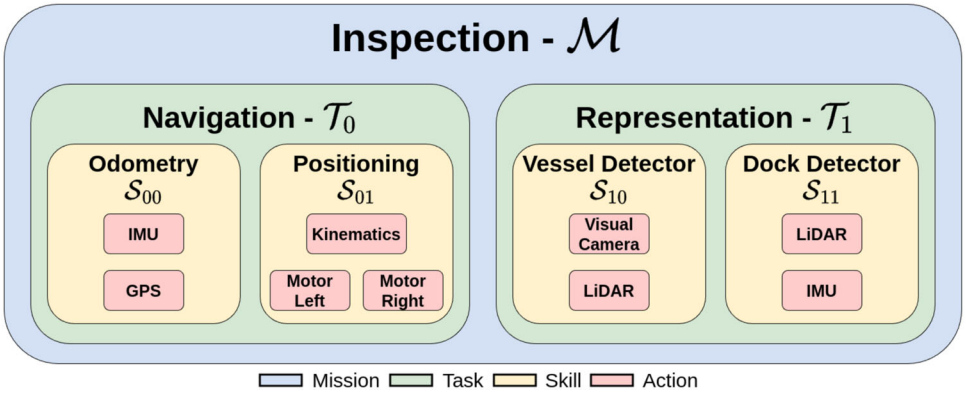


FIGURE 9 Inspection mission using MUSA. Blue, green, yellow, and red boxes represent mission, task, skill, and action layers, respectively. GPS, Global Positioning System; IMU, Inertial Measurement Unit; LiDAR, Light Detection and Ranging; MUSA, Multilayer Universal Software Architecture.

- $\mathcal{M}$—*Inspection*, Topological representation of a predefined area. This requires the tasks:
  - $\mathcal{T}_0$—*Navigation*, drive through a list of goal-points task. This requires the skills:
    - $\mathcal{S}_{00}$—*Odometry*, localization method based on GPS/IMU fusion. It is a persistent skill that is executed continuously. This requires the actions:
      - $\mathcal{A}_{000}$—Get IMU data.
      - $\mathcal{A}_{001}$—Get GPS data.
    - $\mathcal{S}_{01}$—*Positioning*, algorithm based on the error between the current position and the desired waypoint. It is a volatile skill that is executed once until the waypoint position is reached. This requires the actions:
      - $\mathcal{A}_{010}$—Calculate kinematics.
      - $\mathcal{A}_{011}$—Control left motor.
      - $\mathcal{A}_{012}$—Control right motor.
  - $\mathcal{T}_1$—*Representation*, create the topological map task according to the detectors and odometry information. This requires the skills:
    - $\mathcal{S}_{10}$—*Vessel detector*, detection of vessels using LiDAR and visual camera information, providing the object class, bounding box and measure confidence. It is a persistent skill that is executed continuously. This requires the actions:
      - $\mathcal{A}_{100}$—Get visual camera data.
      - $\mathcal{A}_{101}$—Get LiDAR data.
    - $\mathcal{S}_{11}$—*Dock detector*, detection of docks using LiDAR data, providing the dock type and centroid. It is a persistent skill that is executed continuously. This requires the actions:
      - $\mathcal{A}_{110}$—Get LiDAR data.
      - $\mathcal{A}_{111}$—Get IMU data.

The mission $\mathcal{M}$ performs the inspection of the port autonomously creating a semantic topological representation of the surroundings. It is composed of two tasks $\mathcal{T}_0$ and $\mathcal{T}_1$, where the first controls the autonomous navigation in the port and the second creates the representation of the semantic features and vehicle poses.

The task $\mathcal{T}_0$ takes an array of goal-points of undefined size. Each element of that array is composed of three parameters, namely, x, y, and the point's reference frame. This means that coordinates can be expressed in the vehicle's initial odometry frame, or in the Universal Transverse Mercator (UTM) coordinate system. The task layer sends one goal-point at a time to the skill below, and waits for its execution to be completed to send the next command. The pseudocode for this task can be seen in Algorithm 1.

Algorithm 1 Task $\mathcal{T}_0$ procedure

```
while ! T_0.Post-Condition() do
    S_00
end while

for waypoint = 1, ..., i do                          } in parallel
    while ! S_01(x_i, y_i).Post-Condition() do
        S_01(x_i, y_i)
    end while
end for
```

At the skill level, a positioning algorithm ($\mathcal{S}_{01}$) was developed. It receives goal-points as parameters, in the form of 2D coordinates, and outputs linear and angular velocity commands to the action layer. Hence, position is represented by its x, y coordinates, and orientation is expressed by ϕ. Data are driven by the ROS, and localization information is published by an ROS implementation of an Extended Kalman Filter (Moore & Stouch, 2014), which fuses data from a GPS and from an IMU, thus simulating the behavior of $\mathcal{S}_{00}$.

The skill $\mathcal{S}_{01}$ continuous execution state consists of a finite state machine model with five states, namely, an initial state, a rotation phase, a state where the angular velocity is reduced, a cruising state, and a final state, where the ASV's velocity is decreased. The skill's continuous execution behavior is illustrated in Figure 10.

At the initial state, the ASV checks if its position relative to the goal-point is within the limits set by a user defined parameter, which bounds the maximum Euclidean distance—$\|\Delta(x, y)\|_2$—from which the system advances directly to the final state. If $\|\Delta(x, y)\|_2$ is bigger than the defined parameter, the execution state changes to a rotation stage. At this stage, the ASV rotates until it is oriented to the direction given by a line that crosses both the vehicle's baseline and the goal-point. Given

15564967, 2024, 4, Downloaded from https://onlinelibrary.wiley.com/doi/10.1002/rob.22304 by SEA ORCHID (Thailand), Wiley Online Library on [16/02/2026]. See the Terms and Conditions (https://onlinelibrary.wiley.com/terms-and-conditions) on Wiley Online Library for rules of use; OA articles are governed by the applicable Creative Commons License

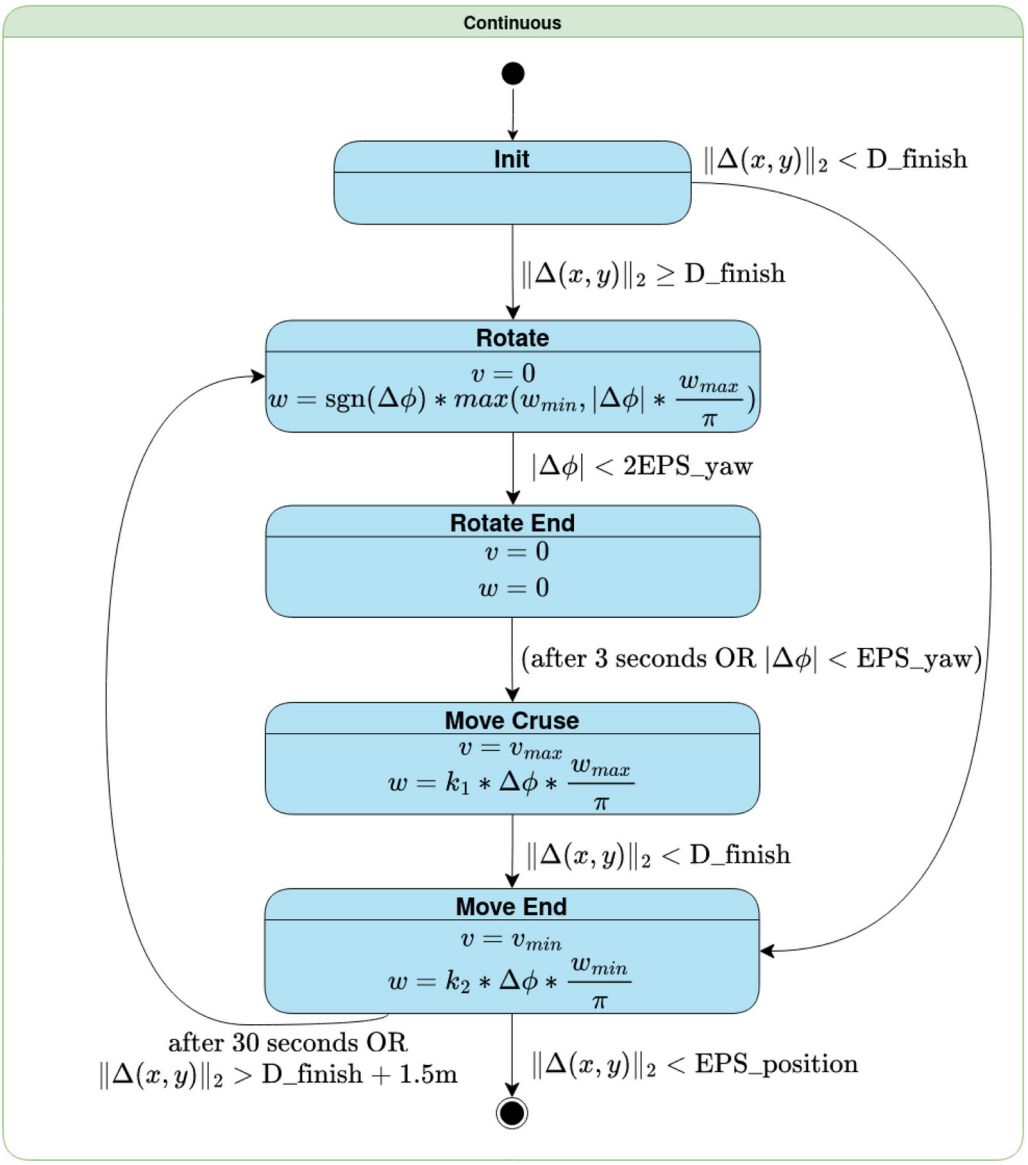


FIGURE 10 The state machine diagram of the continuous execution routine of the proposed positioning skill, $\mathcal{S}_{01}$.

the dynamics of the environment where the ASV operates, and the lack of a finer velocity controller, the ASV stops the rotation when the module of its deviation in orientation—$|\Delta\phi|$—is smaller than a user defined parameter. Then, in the third state, the ASV waits for a time interval to pass, or until the error in orientation reduces in half, to start moving with linear velocity. The time interval duration is, once again, a parameter of the skill that a user can easily set or modify. In the following state, the ASV cruses at the maximum defined linear velocity. The angular velocity is calculated by a proportional controller, with a gain that was tuned during the conducted tests. Finally, as the ASV reaches the goal-points' coordinates, and the skill's continuous execution enters its last stage, linear velocity is reduced to a specified value, and angular velocity is adjusted proportionally to $|\Delta\phi|$.

At the action level, linear and velocity commands sent by the skill are converted into commands for the two electric thrusters, taking into account the kinematics of the ASV through action $\mathcal{A}_{010}$ and providing the velocity command to each motor driver through actions $\mathcal{A}_{011}$ and $\mathcal{A}_{012}$.

The task $\mathcal{T}_1$ takes the odometry from skill $\mathcal{S}_{00}$ and the detections from skills $\mathcal{S}_{10}$ and $\mathcal{S}_{11}$ and creates a semantic topological representation, where the nodes represent the vehicle poses and the semantic features (e.g., docks and vessels) and the edges represent the spatial relationships between them. Odometry nodes describe the vehicle pose and the respective timestamp and feature nodes provide the object pose, velocity, class, timestamp, and detection covariance.

At the skill level, $\mathcal{S}_{10}$ uses the method from Duarte et al. (2022) to detect vessels, where the visual camera data are fed to YOLOv5 to detect the objects and then the LiDAR point cloud is projected over the camera plane, resulting in a range map aligned with the original image. This fusion is used to obtain an enhanced 3D pose of the vessel. Using ROS actions $\mathcal{A}_{100}$ and $\mathcal{A}_{101}$ subscribes the visual camera and LiDAR data. Skill $\mathcal{S}_{11}$ uses the method from Pereira et al. (2021) to

15564967, 2024, 4, Downloaded from https://onlinelibrary.wiley.com/doi/10.1002/rob.22304 by SEA ORCHID (Thailand), Wiley Online Library on [16/02/2026]. See the Terms and Conditions (https://onlinelibrary.wiley.com/terms-and-conditions) on Wiley Online Library for rules of use; OA articles are governed by the applicable Creative Commons License

detect docks within the LiDAR point cloud. After retrieving the point cloud, action $\mathcal{A}_{110}$, the system filters it to remove spurious data and compensate for any undulation using data from the IMU, action $\mathcal{A}_{111}$. Subsequently, the detector segments the point cloud into voxels and employs a neural network to determine whether one or more docks are present in the current frame. If docks are detected, the model classifies them based on their shape.

4 | RESULTS AND APPLICATION

The validation of Nautilus was conducted in accordance with the ATLANTIS technology certification procedures, Figure 11. This rigorous testing framework provides a systematic approach that considers not only the robotic system's characteristics and testing objectives (defined by the Test Center users or end-users), but also the specific task and associated performance indicators. This comprehensive approach ensures that testing results meet the highest standards of reliability, efficiency, and safety (Pinto et al., 2021). The ATLANTIS testing process is specifically designed for entities developing technologies or services related to offshore wind. It aims to validate the demonstrated technology or methodology, ensuring its compliance with existing safety regulations and its viability as a performance-enhancing alternative to traditional methods. The ATLANTIS testing methodology comprises two distinct stages closely linked to the Technology Readiness Level (TRL) of the robotic solution being tested. The first stage, Approval in Principle, involves validations conducted exclusively on the Coastal Testbed. The second stage, Technology Qualification, requires validations on the Offshore Testbed. Obtaining Technology Qualification necessitates the endorsement of external entities (e.g., asset owners). Before proceeding to the Offshore Testbed, a critical step involves validating the technology's deployment and recovery methodologies in the open sea.

The Nautilus successfully completed all testing stages, engaging in four trials at the sites depicted in Figure 12, specifically, the ATLANTIS Test Center and Offshore Trials 1–3, each with varying distances to the shoreline. While TRLs were lower (up to 5), the ASV's performance underwent repeated testing at the ATLANTIS coastal test center (Pinto et al., 2023) situated in the port of Viana do Castelo, Portugal. During the Approval in Principle stage, first trial at the ATLANTIS Test Center, Nautilus reached TRL 6 showcasing its ability to operate in a relevant scenario. During the first offshore trial the deployment methodology was validated in open waters under moderate conditions. For the Technology Qualification stage, two offshore trials were conducted in collaboration with the WFA owners, where Nautilus reached TRL 8. Offshore trial 2 demonstrated deployment near the WFA farm, while offshore trial 3 performed an inspection mission on a WindFloat foundation. To the best of our knowledge, Nautilus became the world's first ASV to perform autonomous tasks on a floating foundation offshore wind farm in the Atlantic. This final trial was conducted at a distance of 18 km from the shoreline, on the WFA wind farm, encountered an estimated H_s during the operation of 1.1 m, and wind velocities averaging 5 m s^{-1}.

The offshore operations happened according to strict safety protocols, especially, related to weather and sea-state conditions: up to 1.5 m of H_s and 10 m s^{-1} of wind speed (ATLANTIS, 2021). All experiments of Nautilus followed a state-of-the-art testing procedure at ATLANTIS Test Center that considers all these parameters and conditions imposed by the industry.

The four trials, namely, ATLANTIS Test Center, Offshore Trial 1, Offshore Trial 2, and Offshore Trial 3, presented varying wind and sea states, and distance to the shoreline, as summarized in Table 3. As can be seen, the validation of Nautilus occurred in

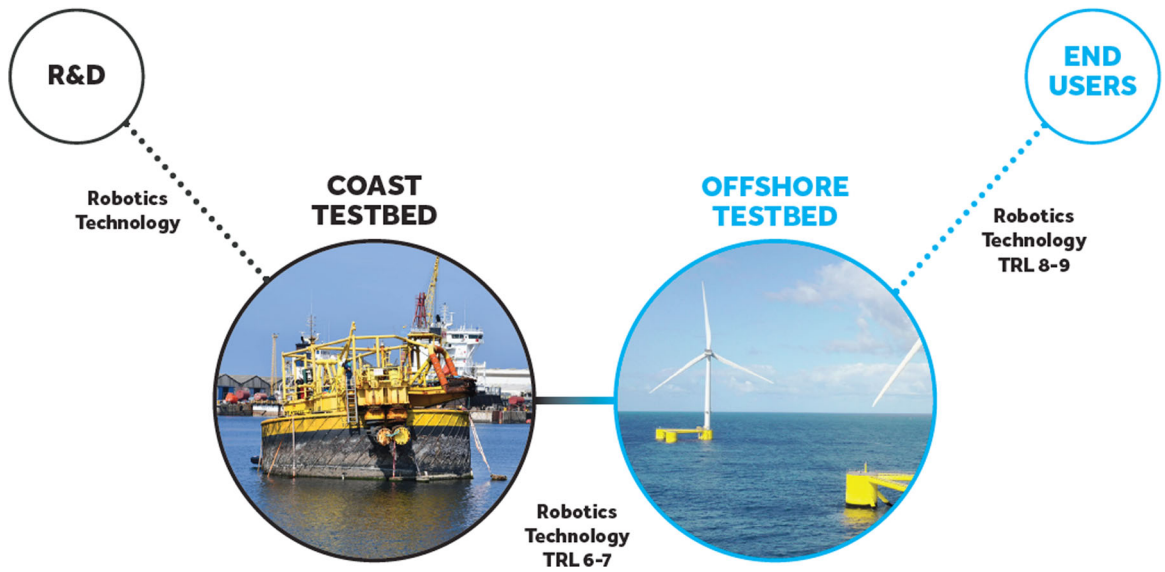


FIGURE 11 ATLANTIS streamline for the validation and demonstration of robotic solutions. R&D, research and development; TRL, Technology Readiness Level.

15564967, 2024, 4, Downloaded from https://onlinelibrary.wiley.com/doi/10.1002/rob.22304 by SEA ORCHID (Thailand), Wiley Online Library on [16/02/2026]. See the Terms and Conditions (https://onlinelibrary.wiley.com/terms-and-conditions) on Wiley Online Library for rules of use; OA articles are governed by the applicable Creative Commons License

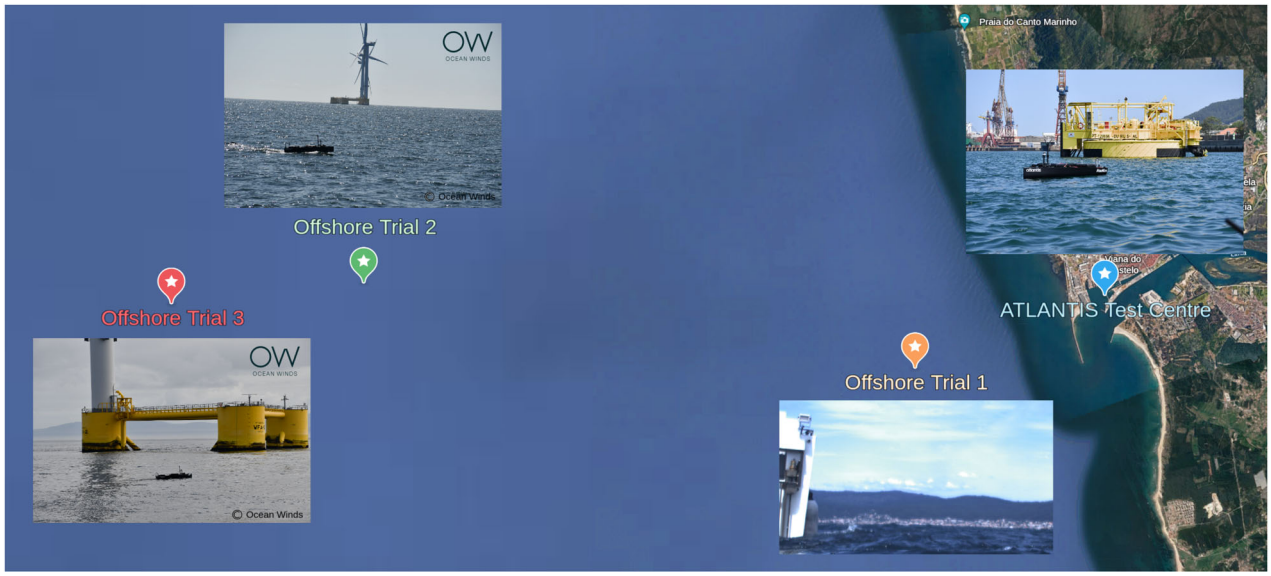


FIGURE 12 Nautilus trial locations in satellite view.

TABLE 3 Summary of the conditions during Nautilus trials.

Trial locations (Figure 12)	Distance from shore (km)	Douglas Sea State	Significant wave height (m)	Wind speed ($m\,s^{-1}$)
ATLANTIS Test Center	–	2	0.2	2–10
Offshore Trial 1	3	4	1.3	10
Offshore Trial 2	14	3	1	7
Offshore Trial 3	18	3	1.1	5

real-world conditions close to the maximum level of sea-state and wind speed allowed by the safety standards followed by the industry.

Nautilus design does not include a keel to facilitate the deployment of this ASV at the sea, and although, it is not expected to operate Nautilus under more challenging weather and sea-state conditions than the industry safety standard, we believe that it would be possible to operate Nautilus up to 1.6 m H_s and wind speed up to 15 $m\,s^{-1}$.

Throughout this section it will be presented an overview of the trials on the near-real and the real environments, presenting the deployment process, tests under different conditions, data samples and application examples.

4.1 | Approval in principle: Near-real environment validation

The ATLANTIS coastal test bed (Pinto et al., 2023) situated on the port of *Viana do Castelo*, Portugal, depicted in Figure 13, served as the venue for all onshore trials throughout the development process and for the Approval in Principle stage. This site comprises the port's infrastructure and the Durius, an offshore floating structure repurposed from the Oil & Gas industry to emulate the floating foundation of the offshore wind energy industry. A video with snippets from some Nautilus trials in this scenario can be found on the link in the footnote.[6]

Nautilus is a portable and deployable system, owing to its compact design. It can be transported on a standard cargo van with a storage space length of at least 3.1 m, a dimension commonly found in vehicles with storage volumes of $10\,m^3$ or more. During transit, a transportation cart is employed, as depicted in Figure 14, with the outboard motors disassembled for ease of handling. The hardware modules can also be detached from their fixation frames, further reducing the overall weight and simplifying transportation tasks for the operator.

At the designated deployment site, the various components and connectors are meticulously assembled and securely fastened, and the power switch is activated to initiate the preliminary safety assessments. The deployment procedure involves the employment of either a crane or an A-frame mechanism, both equipped with a rapid-release snap hook. This snap hook is attached to a 4-point sling that is

[6]MOTION Robotics, 2022. *Nautilus ASV*. URL: https://youtu.be/12niamOnmL8.

15564967, 2024, 4, Downloaded from https://onlinelibrary.wiley.com/doi/10.1002/rob.22304 by SEA ORCHID (Thailand), Wiley Online Library on [16/02/2026]. See the Terms and Conditions (https://onlinelibrary.wiley.com/terms-and-conditions) on Wiley Online Library for rules of use; OA articles are governed by the applicable Creative Commons License

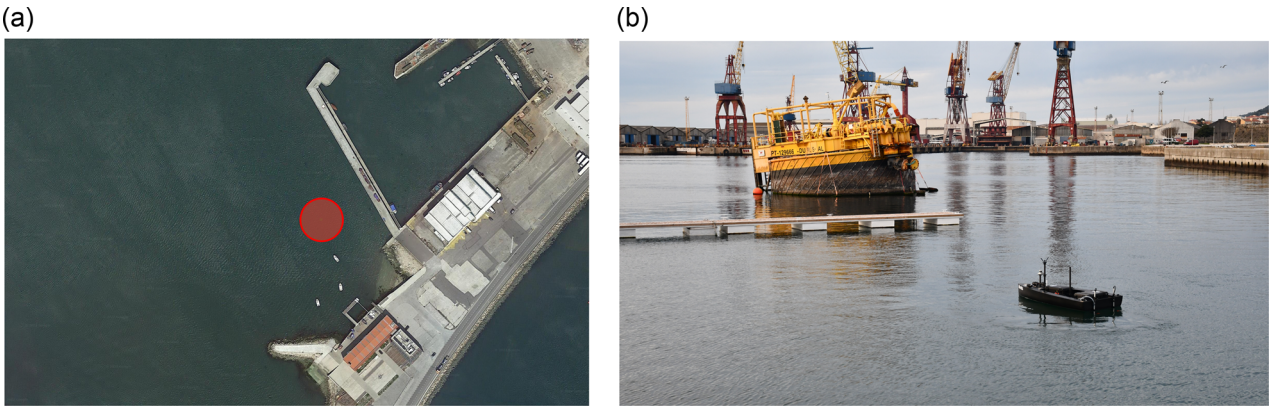


FIGURE 13 The ATLANTIS coastal test center satellite view and shore view. (a) ATLANTIS coastal test bed satellite view. The red circle indicates the floating structure, Durius, approximate location. (b) ATLANTIS coastal test bed shore view.



FIGURE 14 Nautilus on the transportation cart.

connected to Nautilus' ring bolts. This arrangement facilitates the lifting and subsequent controlled descent of Nautilus onto the water's surface, as depicted in Figure 15. The inclusion of the quick-release system eliminates the necessity for a support vessel during the deployment of the ASV. For the recovery phase, a telescopic boat hook complete with a supplementary carabiner support is employed. This apparatus serves to securely attach the winch cable to the previously mentioned sling.

During the trials at the ATLANTIS Test Center, Nautilus was subjected to distinct weather and light conditions to validate the navigational capabilities and the data integrity. Figure 16 depicts three trials under different operational scenarios: clear sky, clouded and night. Nautilus during these trials presented a swift maneuverability allowing to perform quick heading and speed variations due to the hull shape and the differential drive. Despite the absence of environmental waves in *Viana do Castelo* port, it is a high-traffic area for vessels, as such the wake caused by their displacement can cause several ripples with high frequency and heights dependent on the size and velocity of the vehicle, usually with an H_s between 0.1 and 0.2 m. During these trials, Nautilus was affected by this phenomenon showing a high capacity to endure the wake swells, maintaining its structural integrity and safety.

The major effects of the different operational scenarios are noticed on the data acquisition and processing capabilities. Nautilus has a heterogeneous payload capable of acquiring information about the vehicle state and both domains in the maritime environment, namely, surface and underwater, which are affected differently by the conditions. As seen in Figure 4, the data were able to be gathered with high quality with a clear weather. When under low-lighting conditions, the visual cameras images are the most affected requiring higher exposure times, as it can be seen in Figure 17. The use of the LiDAR and thermal camera are complementary to the visual information allowing to operate even at night, since the performance is not affected by the illumination conditions.

The results from the proposed MUSA architecture and the inspection mission implementation are presented and discussed. To provide a metric evaluation of the autonomous navigation task $\mathcal{T}_0$, it was used two different sequences as examples. First, the discussion focuses on a smaller and easier succession of goal-points, and then, a

15564967, 2024, 4, Downloaded from https://onlinelibrary.wiley.com/doi/10.1002/rob.22304 by SEA ORCHID (Thailand), Wiley Online Library on [16/02/2026]. See the Terms and Conditions (https://onlinelibrary.wiley.com/terms-and-conditions) on Wiley Online Library for rules of use; OA articles are governed by the applicable Creative Commons License

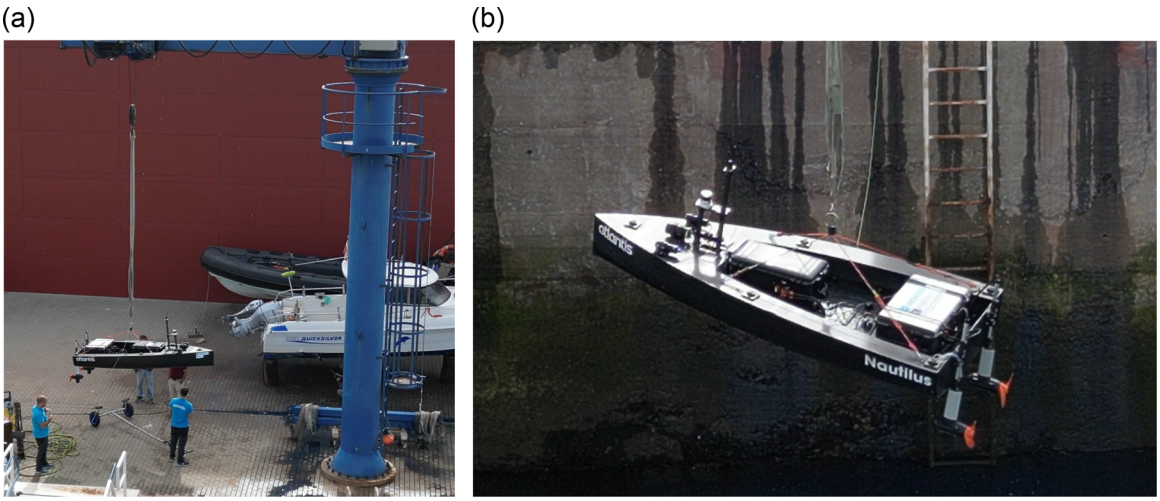


FIGURE 15 Nautilus deployment on port. (a) Nautilus deploy through the ports' crane and (b) Nautilus deploy system close-up.



FIGURE 16 Nautilus trials in the ATLANTIS coastal test center. (a) Nautilus trial with clear weather, (b) Nautilus trial with clouded weather, (c) Nautilus trial at night, and (d) Nautilus trial at night environment conditions.

larger sequence, constrained to harsher environment conditions, such as stronger undulation and wind, is also analyzed. The sample code is publicly available and can be found in https://github.com/edu-goncalves/MUSA. All data was acquired under port conditions. For these experiments, we defined the following parameters:

- A parameter which bounds the maximum $\|\Delta(x, y)\|_2$ from which the system advances directly to the final state. It was set to 2.5 m.
- The maximum allowed deviation in orientation was set to 0.1 rad.
- The maximum allowed deviation in position was set 1 m.

15564967, 2024, 4, Downloaded from https://onlinelibrary.wiley.com/doi/10.1002/rob.22304 by SEA ORCHID (Thailand), Wiley Online Library on [16/02/2026]. See the Terms and Conditions (https://onlinelibrary.wiley.com/terms-and-conditions) on Wiley Online Library for rules of use; OA articles are governed by the applicable Creative Commons License

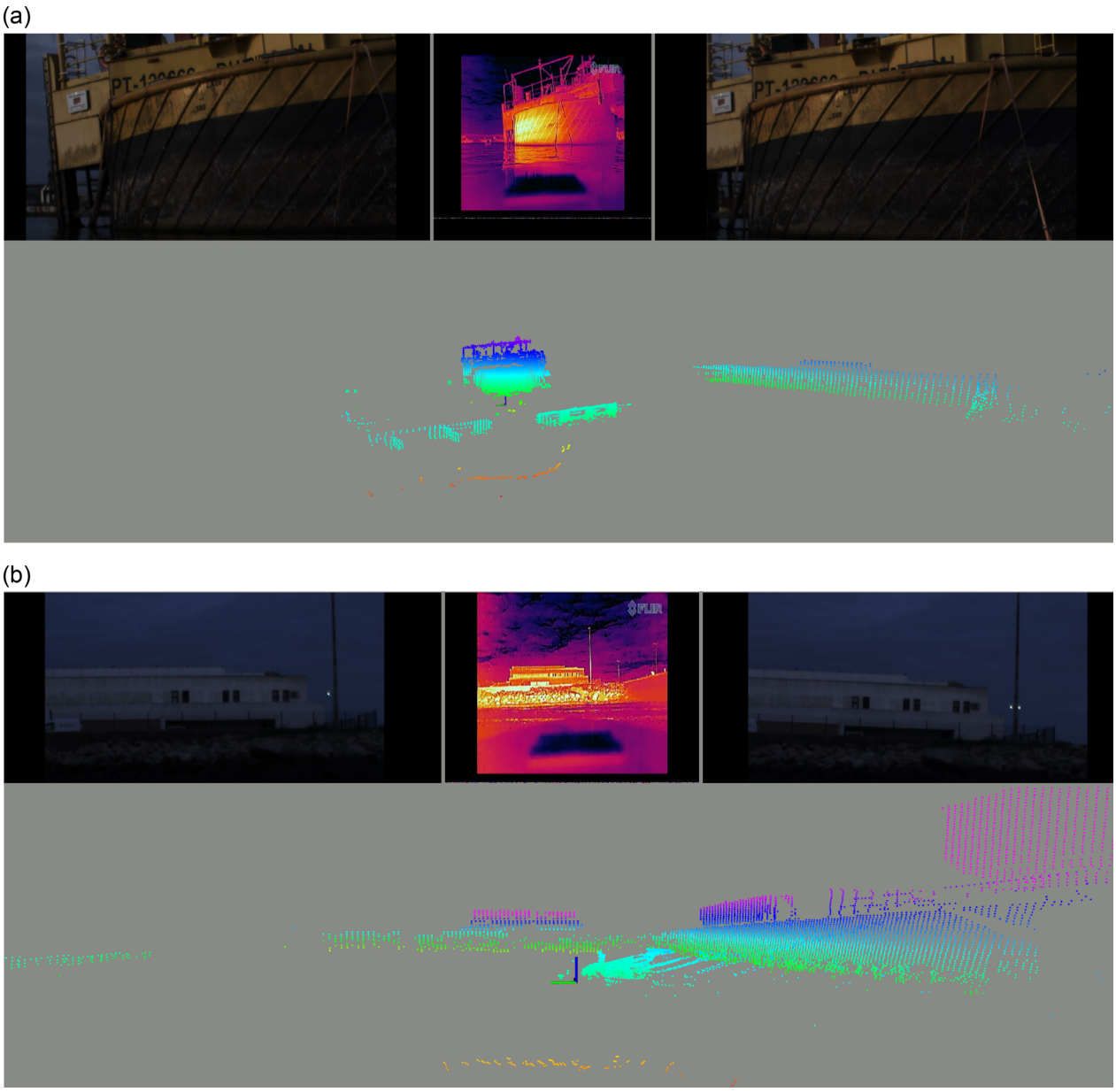


FIGURE 17 Nautilus data sample acquired on different weather conditions. (a) Nautilus data sample acquired on a cloudy day and (b) Nautilus data sample acquired at night.

Pose information was acquired by fusing position data from an RTK-GPS, and orientation data from a 9-axis IMU. Initially, a local odometry frame was defined at the start of the operation. This frame was fixed to the geographic coordinates where the ASV was initialized, hence, the goal-points were expressed in relation to the vehicle's starting pose, forming a set $P^O = \{p_1^O, ..., p_N^O\}$, with $p_n^O = (x_n^O, y_n^O), \forall\, n \in \{1, ..., N\}$, where O superscript represents the fixed odometry coordinate frame. The first experiment consisted of a sequence of the goal-points composed of the set $P^O = \{(5, 0), (15, 10), (10, -5), (5, 0)\}$, and the path followed by the ASV is depicted in Figure 18a. The movement of the vehicle was constrained to a small area, forcing it to rapidly adjust to any deviations in orientation when heading to any of the goal-points. The ASV was initially placed at coordinates (0, 0) on the odometry fixed frame, and started its trajectory oriented to the first goal-point (5, 0), meaning the execution started directly on the cruising state, at maximum linear velocity. Every point, except for the first one, forced the ASV to change its orientation, making sure that every stage of the continuous execution was performed. The ASV was able to successfully execute the task, reaching the 1-m tolerance defined at the beginning of the experiment. A second experiment was conducted, simulating an inspection operation around the structure visible in Figure 13b. As it can be seen in Figure 18b, the scale of the movement was increased, easing constraints on the movement of the vehicle, but exposing it to harsher maritime conditions. The set of goal-points was defined as $P^O = \{(55, -15), (65, 30),(20, 35), (10, -5)\}$, chosen so that the ASV trajectory could circumscribe the Durius floating structure. At the

15564967, 2024, 4, Downloaded from https://onlinelibrary.wiley.com/doi/10.1002/rob.22304 by SEA ORCHID (Thailand), Wiley Online Library on [16/02/2026]. See the Terms and Conditions (https://onlinelibrary.wiley.com/terms-and-conditions) on Wiley Online Library for rules of use; OA articles are governed by the applicable Creative Commons License

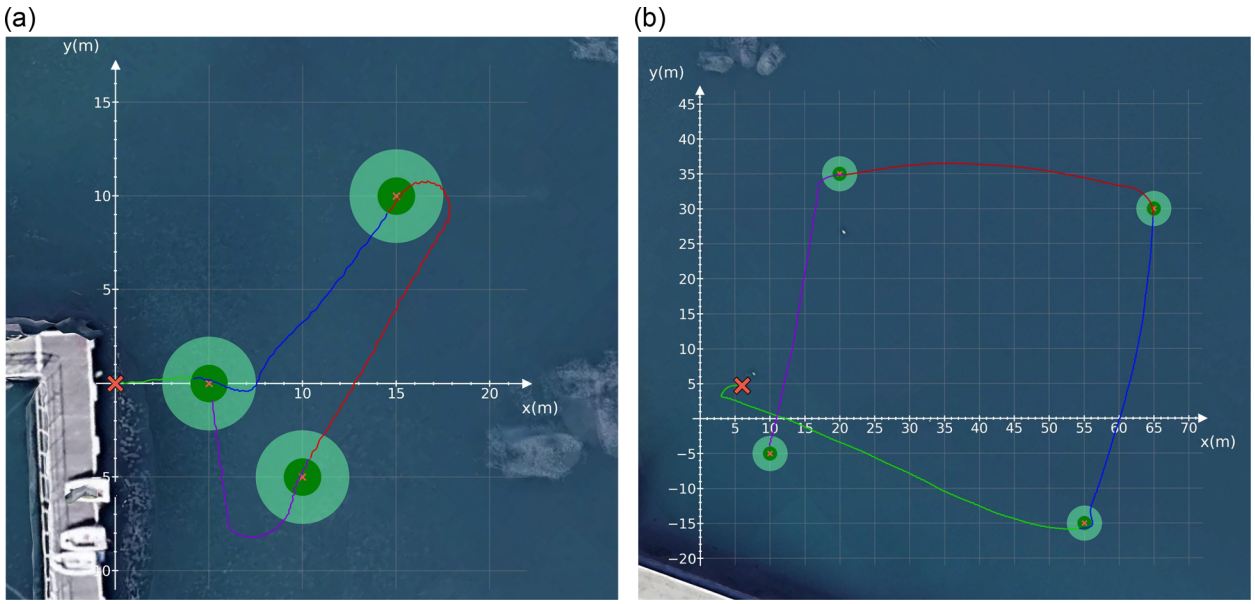


FIGURE 18 Results of task-level experiments performed in a port environment conducted in Viana do Castelo, Portugal. Light green circles represent the distance from the goal-points from which the continuous execution state of the skill enters its last stage, while darker green circles represent the maximum allowed margin of error for the skill to succeed. Each line represents the execution of a single skill. The green line represents the first skill to be executed, followed by a blue, a red, and a purple line. Initial points are marked by a bigger red cross. (a) Task defined by the sequence of goal-points $P^O = \{(5, 0), (15, 10), (10, -5), (5, 0)\}$. (b) Task defined by the sequence of goal-points $P^O = \{(55, -15), (65, 30), (20, 35), (10, -5)\}$.

beginning, and contrarily to the first experiment, the vehicle was placed facing the opposite direction to the first goal-point, with coordinates (6, 5). As it rotated, the vehicle was being dragged by sea currents, as it can be observed in the first segment of the traced trajectory, represented by the green line in Figure 18b. Despite the harsher conditions, the maximum acceptable margins of error were not changed. The task succeeded, meaning the ASV reached every goal-point of the sequence with a maximum error lower than 1 m.

The representation task $\mathcal{T}_1$ was executed within the full mission execution, utilizing the same odometry skill from the navigation task. In this scenario, only the vessel detector skill was employed, as the available docks were not pretrained in the detector. As depicted in Figure 19a, several small boats were docked at the ATLANTIS Test Center. Between the execution of the inspection mission and the capture of the environment picture, some of the vessels shifted positions. The vessel in the purple circle left the inspected area, and a sailboat docked in the green circle area. During the mission, Nautilus (represented by the red ellipsis) navigated around the central dock (indicated by the yellow ellipsis) following the trajectory shown in Figure 19b. The executed mission successfully navigated the ASV near the central docks and detected most of the vessels. An outlier measure (represented by the blue arrow) resulted from a false positive detection provided by the skill $\mathcal{S}_{10}$. Additionally, a vessel was not detected (indicated by the pink arrow) due to an occlusion between the ASV and the vessel during the trajectory segment where it was within line-of-sight.

Thus, the use of Nautilus available sensor payload allows for multiple applications from a simple visualization tool to autonomous navigation and mapping. Figure 20a illustrates the multidomain map of Durius' neighborhood, where the red to purple color scale represents the *Z*-axis variation from minimum to maximum, respectively. For such, a 3D LiDAR odometry, the Continuous-Time Iterative Closest Point (CT-ICP) (Dellenbach et al., 2021), was used to estimate the ASV position given that it was operating in proximity to structures, which allows for a more accurate localization and, then, using the method proposed by Campos, Matos et al. (2021) to reconstruct the multidomain map. As it can be seen, the seafloor representation is sparse (red and orange areas). This is due to the water salinity variation inside the port caused by the mixture between fresh and salt waters that affects the MBES sensor. It causes the sensor to acquire multiechoes and, consequently, spurious data which need to be filtered. During low tide, the MBES sensor detects fewer multiechoes, resulting in a more precise bathymetric reconstruction, as shown in Figure 20b. This enhanced detail is attributed to the reduced occurrence of spurious data from the MBES sensor. Additionally, the soft nature of the seabed further hinders the data acquisition process. To address the challenges of the water salinity and seafloor material, employing an MBES system with a lower operation frequency would provide better swath coverage and enhance the overall data quality.[7]

To verify the adjustment of the multidomain map to the real scenario, the odometry coordinates were aligned with RTK and IMU information, creating a seamless integration with the satellite view, Figure 21. This alignment is demonstrated by the accurate overlapping of the map representation with the static structures in the scenario, including buildings and port infrastructures.

[7]R2Sonic, 2023. *How to Best Use the Multibeam Echosounder Manual*. URL: http://tinyurl.com/mbes-best-practice.

15564967, 2024, 4, Downloaded from https://onlinelibrary.wiley.com/doi/10.1002/rob.22304 by SEA ORCHID (Thailand), Wiley Online Library on [16/02/2026]. See the Terms and Conditions (https://onlinelibrary.wiley.com/terms-and-conditions) on Wiley Online Library for rules of use; OA articles are governed by the applicable Creative Commons License

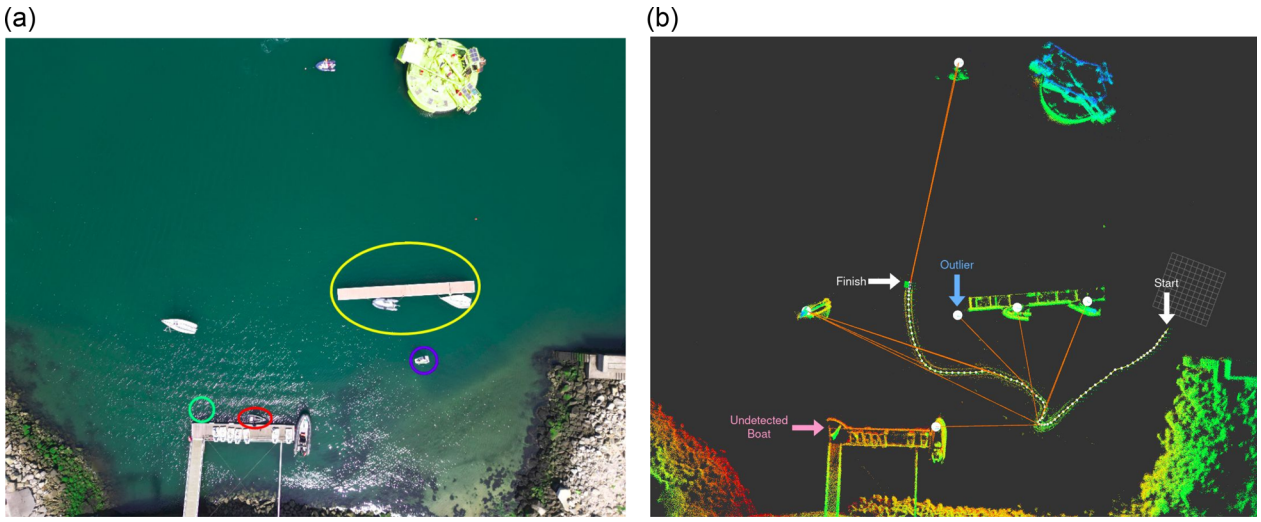


FIGURE 19 Results of the mission performed in a port environment conducted in the ATLANTIS coastal test center with six docked vessels. (a) Approximate conditions of the scenario to be reconstructed and (b) semantic topological representation of the scenario.

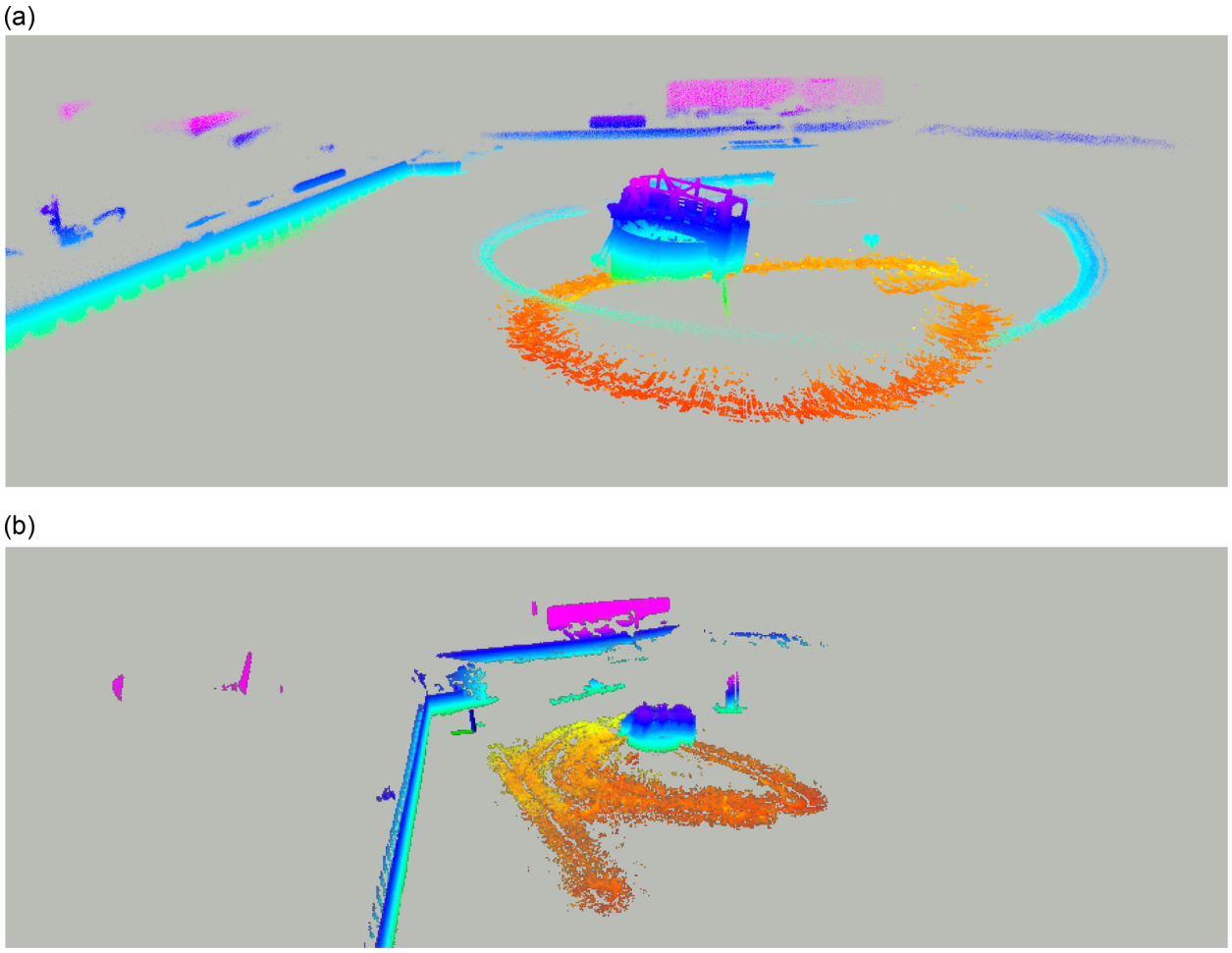


FIGURE 20 Multidomain map created by Nautilus on the ATLANTIS coastal test center with different tide conditions. The red to purple color scale represents the Z-axis variation from minimum to maximum, respectively. (a) Multidomain map created by Nautilus on the ATLANTIS coastal test center and (b) multidomain map created by Nautilus during low tide on the ATLANTIS coastal test center.

15564967, 2024, 4, Downloaded from https://onlinelibrary.wiley.com/doi/10.1002/rob.22304 by SEA ORCHID (Thailand), Wiley Online Library on [16/02/2026]. See the Terms and Conditions (https://onlinelibrary.wiley.com/terms-and-conditions) on Wiley Online Library for rules of use; OA articles are governed by the applicable Creative Commons License

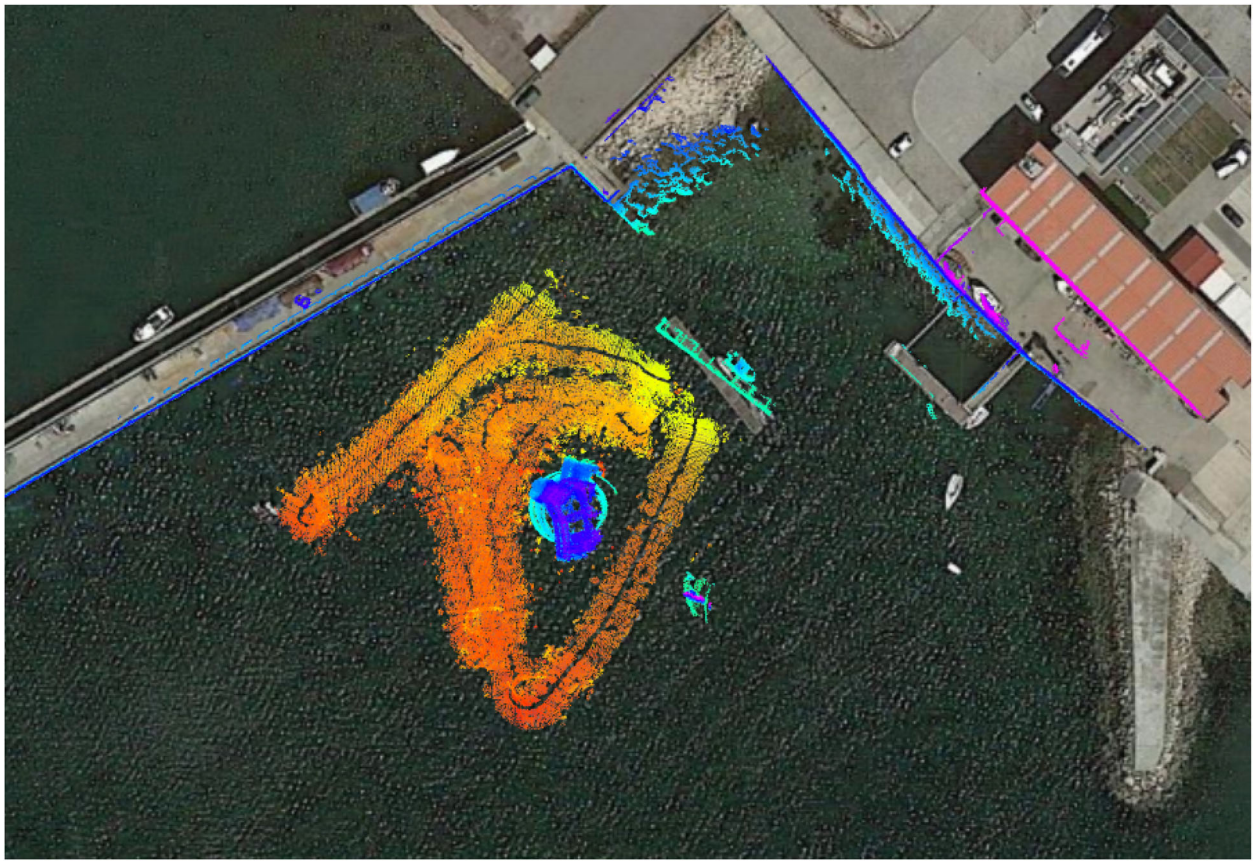


FIGURE 21 Multidomain map with low tide conditions overlap with satellite view. The red to purple color scale represents the Z-axis variation from minimum to maximum, respectively.

Another use case is the positioning system designed according to MUSA, which estimates Nautilus' position through the GPS/IMU fusion and performs a navigation skill to autonomously move from the current position to the mission waypoint and the topological representation of the scenario task. Both constitute the sample inspection mission described. Thus, the vehicle trials allowed to validate the ASV deployability and demonstrated its capacity for executing a vast range of applications due to the data acquisition capabilities and the structural integrity of the hull. Moreover, the design allows for a smooth maneuvering capable of withstanding multiple environmental conditions. To further enhance bathymetric quality, employing a sonar with a lower or adjustable frequency would be beneficial, as it could diminish the influences of water salinity variations and soft seabed conditions, while also expanding the detection range.

4.2 | Technology qualification: Real environment validation

Nautilus successfully completed three offshore trials, spanning varying distances from the shoreline and sea states, as depicted in Figure 12 and summarized in Table 3. The first trial was conducted at 3 km, followed by a second trial at 14 km, and the third and most relevant trial occurred at 18 km within the WFA offshore wind farm. These trials provided a rigorous testing environment to validate and assess the ASV's deployment capabilities and maneuverability under diverse conditions, fulfilling the requirements of the Technology Qualification stage of the ATLANTIS testing process.

The final trial was conducted directly on the WFA wind farm, which comprises three fully operational floating foundations, with a total capacity of 25 MW, Figure 22. The mission was carried out on the farthest turbine from shore, situated approximately 18 km from the coastline, in water depths reaching 100 m.[8]

The deployment in offshore condition follows similar steps as the near-real environment. For safe operations in offshore conditions, stabilizing ropes are used being strategically positioned to mitigate the effects of undulation-induced motion and maintain the stability of Nautilus during its elevation. Figure 23 depicts the deployment procedure of Nautilus adjacent to an offshore wind farm located in *Viana do Castelo*, with operational conditions within the limits for deployment, namely, 1.5 m or less significant wave height (H_s) for small boats (Silva & Estanqueiro, 2013).

[8]WFA, 2023. *WindFloat Atlantic—Offshore wind energy*. URL: https://www.windfloat-atlantic.com/~.

15564967, 2024, 4, Downloaded from https://onlinelibrary.wiley.com/doi/10.1002/rob.22304 by SEA ORCHID (Thailand), Wiley Online Library on [16/02/2026]. See the Terms and Conditions (https://onlinelibrary.wiley.com/terms-and-conditions) on Wiley Online Library for rules of use; OA articles are governed by the applicable Creative Commons License



FIGURE 22 WindFloat Atlantic wind farm.

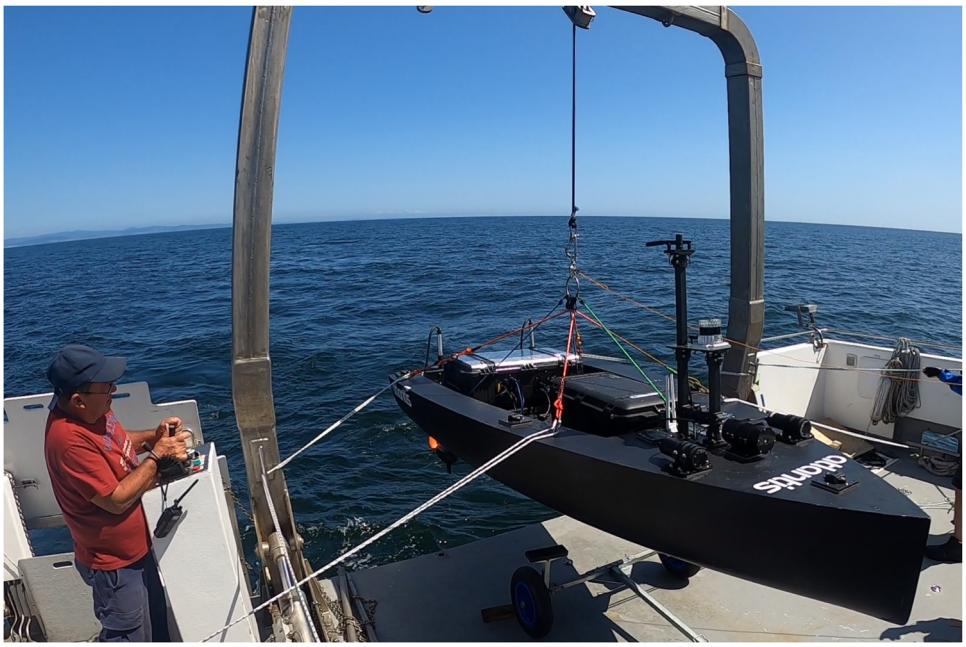


FIGURE 23 Nautilus deployment offshore.

The mission focused on evaluating the comprehensive procedure encompassing the ASV's loading from the port onto the transport vessel Mar Profundo,[9] its on-site preparation, and the subsequent deployment and recovery protocol in open waters. The Nautilus deployment and recovery operation was effectively accomplished in three trials offshore. Figure 24 illustrates the ASV operation during the second and third offshore trials. Moreover, a video of Nautilus operations portraying several applications of Nautilus demonstrated during the Approval in Principle stage, the deployment procedure and segments of the offshore trials during the Technology Qualification stage can be seen in the link on footnote.[10]

[9]INESC TEC, 2022. *Launching of a research ship to test marine technologies*. URL: http://tinyurl.com/mar-profundo.

[10]ATLANTIS Testing Platform for Maritime Robotics, 2023. *Nautilus USV*. URL: http://tinyurl.com/nautilus-off.

15564967, 2024, 4, Downloaded from https://onlinelibrary.wiley.com/doi/10.1002/rob.22304 by SEA ORCHID (Thailand), Wiley Online Library on [16/02/2026]. See the Terms and Conditions (https://onlinelibrary.wiley.com/terms-and-conditions) on Wiley Online Library for rules of use; OA articles are governed by the applicable Creative Commons License

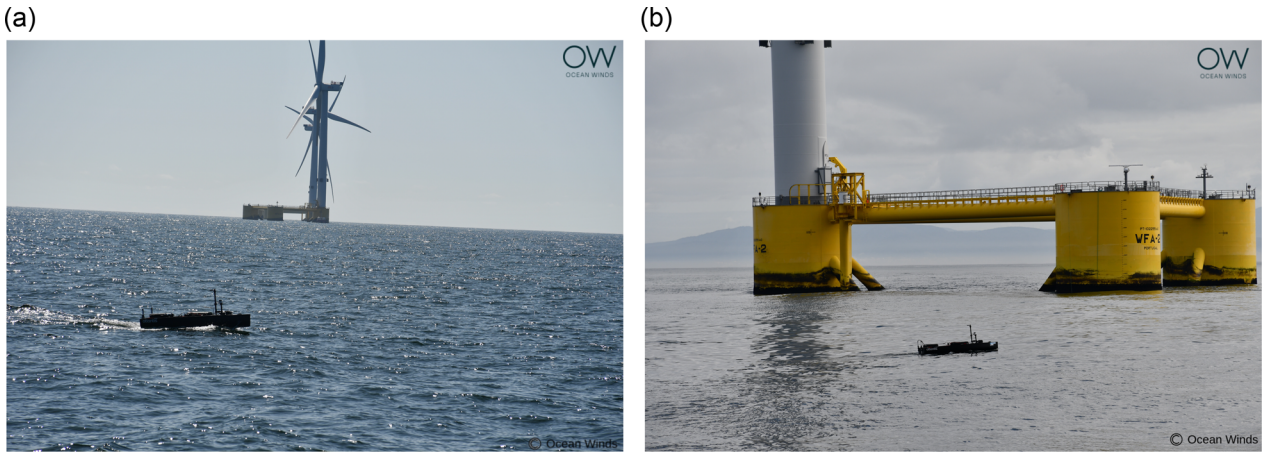


FIGURE 24 Nautilus operations during the second and third offshore trials. (a) Nautilus operating in o shore during the second trial and (b) Nautilus operating in o shore during the third trial.

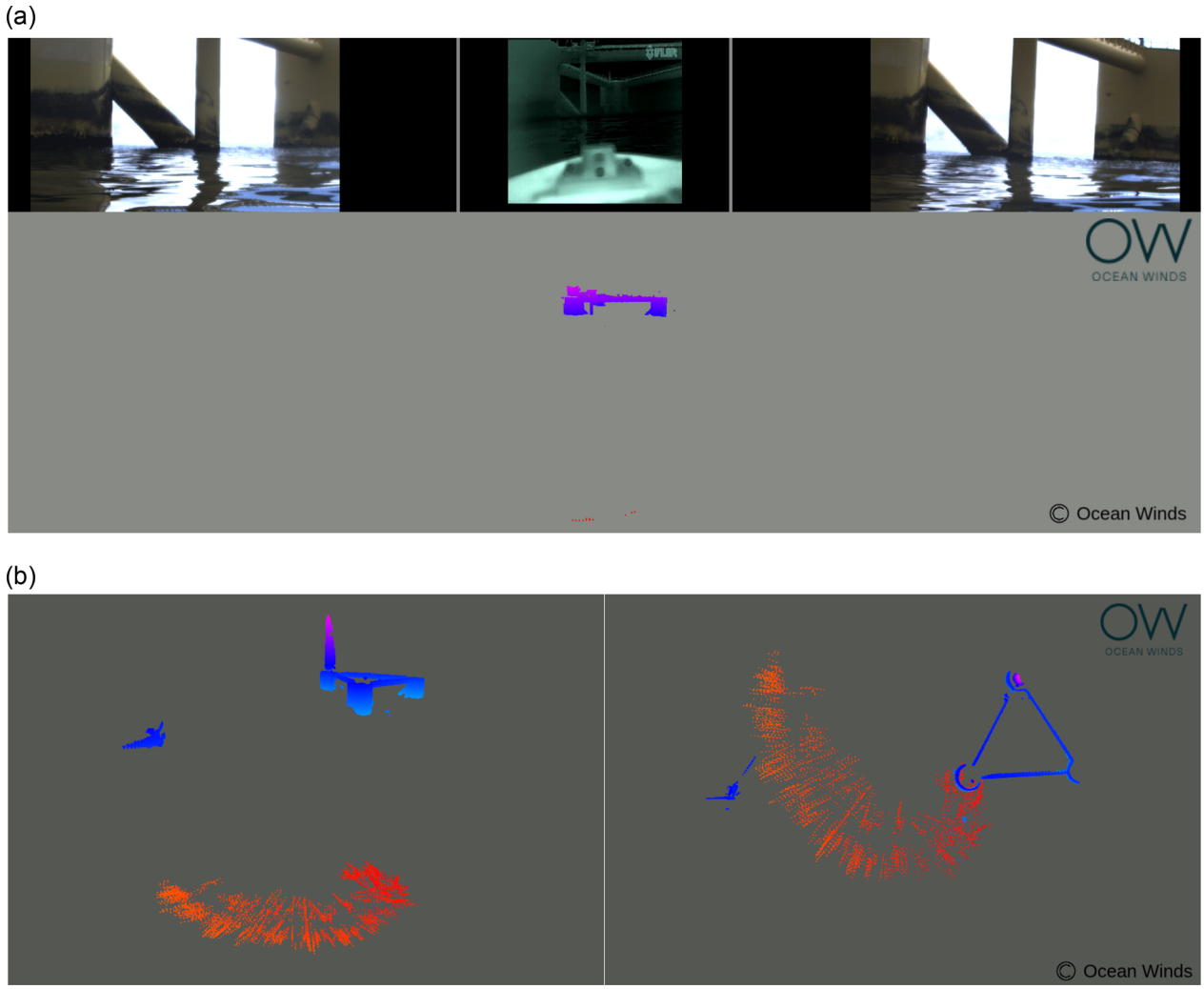


FIGURE 25 Nautilus data sample and multidomain map gathered during the third offshore trial. (a) Nautilus data sample acquired on the Windfloat Atlantic wind farm and (b) multidomain map of the Windfloat Atlantic offshore wind farm.

15564967, 2024, 4, Downloaded from https://onlinelibrary.wiley.com/doi/10.1002/rob.22304 by SEA ORCHID (Thailand), Wiley Online Library on [16/02/2026]. See the Terms and Conditions (https://onlinelibrary.wiley.com/terms-and-conditions) on Wiley Online Library for rules of use; OA articles are governed by the applicable Creative Commons License

In the near future, automatized deployment and recovery mechanisms for small ASV such as Nautilus need to be established to foster uncrewed O&M operations and to increase wave height limitation for the O&M operations.

During the offshore trials, the ASV demonstrated structural integrity and safety, operating under significant wave height (H_s) conditions of up to 1.3 m. Figure 25a presents a sample of the data gathered during the third trial, which is highlighted in Figure 24b. As shown, the LiDAR, visual, and thermal cameras provided distinctive data from the floating foundation. However, the MBES returned highly sparse data with a low quantity of valid beams. This is due to the sensor's range limitation of 100 m, which is insufficient to capture the seafloor, which is estimated to be deeper than 96 m in the trial zone, according to the Portuguese Navy Hydrographic Institute charts.[11] The multidomain map of the Windfloat foundation, as depicted in Figure 25b, was generated using the data gathered during Offshore Trial 3. A comprehensive reconstruction of the emersed domain of the foundation was achieved employing LiDAR data, obtained with the CT-ICP LiDAR-based odometry algorithm, as it was operating in proximity to structures. This allows for a more accurate and robust localization and, then, used the method proposed by Campos, Matos et al. (2021) to reconstruct the multidomain map of the offshore wind turbine foundation, providing a complete representation for the splashing zone and the seafloor.

5 | CONCLUSION

This work presented the design of an ASV for offshore wind farms inspection, called Nautilus, and enables the operation in offshore with moderate wave conditions (up to 2.5 m), while providing multimodal data that enable the navigation and perception of the surroundings. Both its hardware and software are modular, where a multilayer software architecture divided into four distinct layers (mission, task, skill, and action) is used to build the software architecture. This provides a flexible structure to describe a mission as a set of tasks with different skills performing several actions, as well as a unified software architecture for O&M operations. Its design fully describes the complexity levels for controlling the vehicle, going from the low-level system actuation to complex high-level configurations, while maintaining an abstraction from the hardware. Nautilus was designed to operate within the safety standards of the O&M industry for Ocean Winds, namely, the maximum significant weight of 1.5 m (Douglas Sea State 4) and wind speeds of 10 m s^{-1}.

Extensive trials on the ATLANTIS coastal test bed demonstrated Nautilus deployability and capacity to smoothly navigate and data acquisition capabilities, even with different weather conditions. As well, the hardware architecture allows an external communication with an SCC through Wi-Fi, operates even BVLOS, and, even, uses the sensor payload for multiple applications, such as mapping or night missions. The multimodal sensor payload enables the creation of 3D multidomain maps of the scenario, which seamlessly overlay with satellite imagery. This comprehensive representation facilitates the inspection of infrastructure components, such as the scour protection condition and the structural integrity of the splashing zone. Nautilus' software design also provided an easy architecture to adapt to different vehicles requiring only to modify the actions layer to the available hardware.

The ATLANTIS testing process was used in all demonstrations and validations with Nautilus in near-real and real environments. The ASV deployment procedures and navigability of Nautilus were validated under distinct environmental conditions, namely, a Douglas Sea State up to 4 and wind speeds up to 10 m s^{-1}, within the O&M industry safety standards. This process allowed the vehicle to reach a TRL 8 through the demonstration to the end-users on the WFA offshore wind farm. As such, Nautilus became the first ASV to perform autonomously on a floating offshore wind farm in the Atlantic.

[11]Hydrographic Institute, 2023. *Hidrográfico Mais*. URL: http://tinyurl.com/geomarhidro.

ACKNOWLEDGMENTS

This work is partly funded by the Portuguese Government through the FCT—Foundation for Science and Technology within the Ph.D. studentships SFRH-BD-144263-2019 (to Daniel F. Campos) and 2021.05561.BD (to Maria I. Pereira), and by the European Union's Horizon 2020—The EU Framework Programme for Research and Innovation 2014–2020, under grant agreement No. 871571 (ATLANTIS). The authors are thankful to Ocean Winds for providing access to the WindFloat Atlantic offshore wind farm and the support throughout the validation procedures.

ORCID

Daniel F. Campos https://orcid.org/0000-0002-3982-1856

REFERENCES

Agostinho, L.R., Ricardo, N.M., Pereira, M.I., Hiolle, A. & Pinto, A.M. (2022) A practical survey on visual odometry for autonomous driving in challenging scenarios and conditions. *IEEE Access*, 10, 72182–72205.

Albore, A., Doose, D., Grand, C., Lesire, C. & Manecy, A. (2021) Skill-based architecture development for online mission reconfiguration and failure management. In: *2021 IEEE/ACM 3rd International Workshop on Robotics Software Engineering (RoSE)*, Madrid, Spain. IEEE, pp. 47–54.

Albrechtsen, E. (2012) Occupational safety management in the offshore windindustry-status and challenges. *Energy Procedia*, 24, 313–321.

ATLANTIS. (2021) *Survey on legal and regulatory specifications for IMR robots operating in offshore wind farms*. Meyrin, Switzerland: Zenodo. Available from: https://doi.org/10.5281/zenodo.5042754

Brooks, R. (1986) A robust layered control system for a mobile robot. *IEEE Journal on Robotics and Automation*, 2(1), 14–23.

Campos, D.F., Matos, A. & Pinto, A.M. (2019) An adaptive velocity obstacle avoidance algorithm for autonomous surface vehicles. In: *2019 IEEE/RSJ International Conference on Intelligent Robots and Systems (IROS), Macau, China*. IEEE, pp. 8089–8096.

15564967, 2024, 4, Downloaded from https://onlinelibrary.wiley.com/doi/10.1002/rob.22304 by SEA ORCHID (Thailand), Wiley Online Library on [16/02/2026]. See the Terms and Conditions (https://onlinelibrary.wiley.com/terms-and-conditions) on Wiley Online Library for rules of use; OA articles are governed by the applicable Creative Commons License

Campos, D.F., Matos, A. & Pinto, A.M. (2020) Multi-domain mapping for offshore asset inspection using an autonomous surface vehicle. In: *2020 IEEE International Conference on Autonomous Robot Systems and Competitions (ICARSC), Ponta Delgada, Portugal*. IEEE, pp. 221–226.

Campos, D.F., Matos, A. & Pinto, A.M. (2021) Multi-domain inspection of offshore wind farms using an autonomous surface vehicle. *SN Applied Sciences*, 3, 455.

Campos, D.F., Matos, A. & Pinto, A.M. (2022) Modular multi-domain aware autonomous surface vehicle for inspection. *IEEE Access*, 10, 113355–113375.

Campos, D.F., Pereira, M., Matos, A. & Pinto, A.M. (2021) DIIUS—distributed perception for inspection of aquatic structures. In: *OCEANS 2021*, San Diego, CA, USA. IEEE, pp. 1–5.

Civera, M. & Surace, C. (2022) Non-destructive techniques for the condition and structural health monitoring of wind turbines: a literature review of the last 20 years. *Sensors*, 22(4), 1627.

Claro, R., Silva, R. & Pinto, A. (2020) Detection and mapping of monopiles in offshore wind farms using autonomous surface vehicles. In: *Global Oceans 2020: Singapore–U.S. Gulf Coast, Biloxi, MS, USA*. IEEE, pp. 1–4.

Cui, Y., Osaki, S. & Matsubara, T. (2021) Autonomous boat driving system using sample-efficient model predictive control-based reinforcement learning approach. *Journal of Field Robotics*, 38(3), 331–354.

Curto, D., Franzitta, V. & Guercio, A. (2021) Sea wave energy. A review of the current technologies and perspectives. *Energies*, 14(20), 6604.

Dellenbach, P., Deschaud, J. E., Jacquet, B. & Goulette, F. (2022) CT-ICP: real-time elastic liDAR odometry with loop closure. In: *2022 International Conference on Robotics and Automation (ICRA), Philadelphia, PA, USA*, pp. 5580–5586. Available from: https://doi.org/10.1109/ICRA46639.2022.9811849

Duarte, D.F., Pereira, M.I. & Pinto, A.M. (2022) Multiple vessel detection in harsh maritime environments. *Marine Technology Society Journal*, 56, 58–67

Eudeline, G. (2019) Drix USV—improving safety and margins through efficient data acquisition. In: *Abu Dhabi International Petroleum Exhibition & Conference, Abu Dhabi, UAE*. Society of Petroleum Engineers.

Ferreira, H., Almeida, C., Martins, A., Almeida, J., Dias, N., Dias, A. & Silva, E. (2009) Autonomous bathymetry for risk assessment with ROAZ robotic surface vehicle. In: *OCEANS 2009-EUROPE, Bremen, Germany*. IEEE, pp. 1–6.

Han, J., Cho, Y., Kim, J., Kim, J., Son, N.-s. & Kim, S.Y. (2020) Autonomous collision detection and avoidance for ARAGON USV: development and field tests. *Journal of Field Robotics*, 37(6), 987–1002.

Hasegawa, T., Suehiro, T. & Takase, K. (1992) A model-based manipulation system with skill-based execution. *IEEE Transactions on Robotics and Automation*, 8(5), 535–544

Huang, P.-C., Hsieh, Y.-H. & Mok, A.K. (2018). A skill-based programming system for robotic furniture assembly. In: *2018 IEEE 16th International Conference on Industrial Informatics (INDIN)*, Porto, Portugal. IEEE, pp. 355–361.

Kyrarini, M., Haseeb, M.A., Ristić-Durrant, D. & Gräser, A. (2019) Robot learning of industrial assembly task via human demonstrations. *Autonomous Robots*, 43(1), 239–257.

Lee, D.G., Oh, S. & Son, H.I. (2016) Maintenance robot for 5-mw offshore wind turbines and its control. *IEEE/ASME Transactions on Mechatronics*, 21(5), 2272–2283

Leite, A., Pinto, A.M. & Matos, A. (2018) A safety monitoring model for a faulty mobile robot. *Robotics*, 7(3), 32.

Leite, P.N. & Pinto, A.M. (2024) Fusing heterogeneous tri-dimensional information for reconstructing submerged structures in harsh sub-sea environments. *Information Fusion*, 103, 102126.

Moore, T. & Stouch, D. (2014) A generalized extended Kalman filter implementation for the robot operating system. In: Menegatti, E., Michael, N., Berns, K. & Yamaguchi, H. (Eds.) *Proceedings of the 13th International Conference on Intelligent Autonomous Systems (IAS-13)*. Cham, Switzerland: Springer International Publishing.

Neves, F.S., Campos, H.J., Campos, D.F., Claro, R.M., Almeida, P.N., Marques, J.V. & Pinto, A.M. (2023) Shore control centre for multi-domain heterogeneous robotic vehicles. In: *OCEANS 2023*, Limerick, Ireland. IEEE, pp. 1–4.

Papadopoulos, G., Kurniawati, H., Shariff, A.S.B.M., Wong, L.J. & Patrikalakis, N.M. (2014) Experiments on surface reconstruction for partially submerged marine structures. *Journal of Field Robotics*, 31(2), 225–244.

Pedersen, M.R., Nalpantidis, L., Andersen, R.S., Schou, C., Bøgh, S., Krüger, V. & Madsen, O. (2016) Robot skills for manufacturing: from concept to industrial deployment. *Robotics and Computer-Integrated Manufacturing*, 37, 282–291.

Pereira, M.I., Claro, R.M., Leite, P.N. & Pinto, A.M. (2021) Advancing autonomous surface vehicles: a 3D perception system for the recognition and assessment of docking-based structures. *IEEE Access*, 9, 53030–53045.

Pinto, A.M., Amorim Marques, J.V., Abreu, N., Campos, D.F., Inês Pereira, M., Gonçalves, E., Campos, H.J., Pereira, P., Neves, F., Matos, A., Govindaraj, S. & Durand, L. (2023) ATLANTIS coastal testbed: a near-real playground for the testing and validation of robotics for O&M. In: *OCEANS 2023*, Limerick, Ireland. IEEE, pp. 1–5.

Pinto, A.M., Marques, J.V.A., Campos, D.F., Abreu, N., Matos, A., Jussi, M., Berglund, R., Halme, J., Tikka, P., Formiga, J., Verrecchia, C., Langiano, S., Santos, C., Sá, N., Stoker, J.-J., Calderoni, F., Govindaraj, S., But, A., Gale, L.... Aceto, L. (2021) ATLANTIS—the Atlantic testing platform for maritime robotics. In: *OCEANS 2021: San Diego-Porto*, pp. 1–5.

Pinto, A.M. & Matos, A.C. (2020) MARESye: a hybrid imaging system for underwater robotic applications. *Information Fusion*, 55, 16–29.

Plueddemann, A.J., Kukulya, A.L., Stokey, R. & Freitag, L. (2012) Autonomous underwater vehicle operations beneath coastal sea ice. *IEEE/ASME Transactions on Mechatronics*, 17(1), 54–64.

Plumet, F., Pêtrès, C., Romero-Ramirez, M.-A., Gas, B. & Ieng, S.-H. (2015) Toward an autonomous sailing boat. *IEEE Journal of Oceanic Engineering*, 40(2), 397–407.

Quigley, M., Conley, K., Gerkey, B., Faust, J., Foote, T., Leibs, J., Wheeler, R. & Ng, A. (2009) ROS: an open-source robot operating system. In: ICRA Workshop on Open Source Software. Vol. 3.

Schou, C., Andersen, R.S., Chrysostomou, D., Bøgh, S. & Madsen, O. (2018) Skill-based instruction of collaborative robots in industrial settings. *Robotics and Computer-Integrated Manufacturing*, 53, 72–80.

Silva, N. & Estanqueiro, A. (2013) Impact of weather conditions on the windows of opportunity for operation of offshore wind farms in Portugal. *Wind Engineering*, 37(3), 257–268.

Silva, R., Matos, A. & Pinto, A.M. (2022) Multi-criteria metric to evaluate motion planners for underwater intervention. *Autonomous Robots*, 46, 971–983.

Teng, M., Ye, L., Yuxin, Z., Yanqing, J., Qianyi, Z. & Pascoal, A.M. (2021) Efficient bathymetric SLAM with invalid loop closure identification. *IEEE/ASME Transactions on Mechatronics*, 26(5), 2570–2580.

Wang, W., Gheneti, B., Mateos, L.A., Duarte, F., Ratti, C. & Rus, D. (2019) Roboat: an autonomous surface vehicle for urban waterways. In: *2019 IEEE/RSJ International Conference on Intelligent Robots and Systems (IROS)*, Macau, China. IEEE, pp. 6340–6347.

Wang, W., Mateos, L.A., Park, S., Leoni, P., Gheneti, B., Duarte, F., Ratti, C. & Rus, D. (2018). Design, modeling, and nonlinear model predictive tracking control of a novel autonomous surface vehicle. In: *2018 IEEE International Conference on Robotics and Automation (ICRA)*, Brisbane, QLD, Australia. IEEE, pp. 6189–6196.

15564967, 2024, 4, Downloaded from https://onlinelibrary.wiley.com/doi/10.1002/rob.22304 by SEA ORCHID (Thailand), Wiley Online Library on [16/02/2026]. See the Terms and Conditions (https://onlinelibrary.wiley.com/terms-and-conditions) on Wiley Online Library for rules of use; OA articles are governed by the applicable Creative Commons License

Wang, L., Zhang, Z. & Luo, X. (2019) A two-stage data-driven approach for image-based wind turbine blade crack inspections. *IEEE/ASME Transactions on Mechatronics*, 24(3), 1271–1281.

Wolf, M.T., Assad, C., Kuwata, Y., Howard, A., Aghazarian, H., Zhu, D., Lu, T., Trebi-Ollennu, A. & Huntsberger, T. (2010) 360-Degree visual detection and target tracking on an autonomous surface vehicle. *Journal of Field Robotics*, 27(6), 819–833.

How to cite this article: Campos, D.F., Gonçalves, E.P., Campos, H.J., Pereira, M.I. & Pinto, A.M. (2024) Nautilus: an autonomous surface vehicle with a multilayer software architecture for offshore inspection. *Journal of Field Robotics*, 41, 966–990. https://doi.org/10.1002/rob.22304

15564967, 2024, 4, Downloaded from https://onlinelibrary.wiley.com/doi/10.1002/rob.22304 by SEA ORCHID (Thailand), Wiley Online Library on [16/02/2026]. See the Terms and Conditions (https://onlinelibrary.wiley.com/terms-and-conditions) on Wiley Online Library for rules of use; OA articles are governed by the applicable Creative Commons License